InnoVationinfo International Journal of Nano Research

ISSN: 2581-6608
Volume 8: 1
Int J Nano Rech 2025

Development an Innovative, Contrarian and Unprecedented Theragnostic Technology based on Submicron Fluorescent Diamond Particles, FDP-NV-750NM Coated with Doxorubicin and Duplex Sorafenib. PART II: - In Vivo Proof of Hypotheses and Technical Feasibility for Direct to Tumor Injection of FDP-NV-DOX~SOR to Xenograft Tumors in Immune Compromised BALB/C2 'NUDE' Mice

Feuerstein GZ*[1]
Firestein R[2]
Marcinkiewicz C[1,3]

[1]*FARMACON LLC, San Diego, California, USA*
[2]*College of Engineering, Temple University, Philadelphia PA, USA*
[3]*Department of Molecular and Translational Sciences, Centre for Cancer Research, Hudson Institute of Medical Research, Monash University Clayton, Victoria 3168, Australia*

Abstract

Purpose: To evaluate doxorubicin (DOX)-coated fluorescent diamonds particles FDP-NV-750nm (FDP-DOX) for its potential to serve for therapeutic and imaging of hepatocellular cancer (HCC) in BALB/c nude mice.

Methods: Human liver cancer-cell line (Hep-3B-luc) was used to induce a subcutaneous tumor in the right auxiliary space of BALB/c 'nude' mice. HCC tumors' progression was evaluated in vivo by caliper measurements vetted by MRI, and bioluminescence of Hep-3B-luc, generated by a single intravenous injection of luciferin. Bioluminescence was monitored extracorporeally by *in vivo* Imaging System (IVIS) at Ex/Em of 680/740nm, respectively. FDP-NV-750nm (+/- DOX) injected directly into tumors were monitored by NIR emanating from FDP-NV-750 deposited in the tumor. Paraffin blocks of frozen tumors were preserved and sliced at 4-5 um for histological inspection. Immunohistochemistry is used for Alpha-FETO Protein (AFP), a standard biomarker of liver cancer cells. Liver macrophage cells were illustrated with monoclonal antibodies targeting CD68+. Hematoxylin/Eosin (H&E) and DAPI stained was used for cells' nuclei in support of high-density quantitative cells counts. Light diffraction microscopy was used for validation of the location of FDP-NV-750nm deposited in tumors, and further on, fluorescence emission microscopy for NIR emission as proxy biomarker of FDP-NV. To confirm desorption of doxorubicin and formation of its metabolite, doxorubicinol, tumors were isolated and stored frozen. Doxorubicin and its metabolite doxorubicinol, were extracted at WuXiAppTec, chemical division, China. The chemotherapeutic "payload (DOX) and subjected to gas chromatography (GC) followed by mass spectrometry (MS/MS). Mice body weights and thriving behavior were inspected periodically by trained veterinarians according to FDA regulatory guidance. Bioluminescence generated by engineered Hep-3B-luc cells was induced by injection of luciferin served as biomarker for cancer cells viability. Euthanasia was performed in mice cages using 5% isoflurane in oxygen. Sorafenib impact on Hep-3B-luc was tested in vitro in the same Hep-3B-luc cells.

Results: Each of the control groups displayed exponential growth of

Article Information

Article Type: Research article
Article Number: IJNR131
Received Date: 02 February, 2025
Accepted Date: 19 May, 2025
Published Date: 26 May, 2025

***Corresponding author:** Feuerstein GZ, FARMACON LLC, San Diego, California, USA.

Citation: Feuerstein GZ, Firestein R, Marcinkiewicz C (2025) Development an Innovative, Contrarian and Unprecedented Theragnostic Technology based on Submicron Fluorescent Diamond Particles, FDP-NV-750NM Coated with Doxorubicin and Duplex Sorafenib. PART II: - In Vivo Proof of Hypotheses and Technical Feasibility for Direct to Tumor Injection of FDP-NV-DOX~SOR to Xenograft Tumors in Immune Compromised BALB/C2 'NUDE' Mice. Int J Nano Rech Vol: 8, Issu: 1 (01-19).

tumors and no difference was found between vehicle control (PBS) and FDP-NV-750 (naive) groups. FDP-DOX treated tumors displayed modest mitigation of tumors' growth; however, in combination with SOR (sorafenib, duplex treatment) significantly enhanced efficacy (tumor growth or bioluminescence) as compared to either of the control's groups ($p<0.0001$, N=5). Bio-fluorescence generated by Hep-3B-luc cancer cells exposed to luciferin infusion was reduced by 53.8% by FDP-DOX treated mice ($p<0.0001$, N=8) Vs either of the controls). Doxorubicin was detected in each tumor (mouse) treated by FDP-DOX.

Conclusion: The data presented in this manuscript strongly suggest that FDP-NV-750 nm coated by doxorubicin or in duplex with sorafenib (FDP-DOX-75ug/mg+sorafenib) might serve as a novel therapeutic modality for direct to tumors injections via Trans-arterial delivery. Our data also suggest that higher doses delivered over extended time by repeated courses might gain higher efficacy in a duplex format and possibly could realize "overall survival" outcome, (which was not an objective of the present study but an ultimate goal for future development). Our data is the first in its kind to demonstrate that a non-nano diamond particle carrying chemotherapeutics (DOX) enhances efficacy while omitting embolectomy altogether. FDP-DOX-DOX+SOR is envisioned to deliver synergy as well illumination of the locoregional (NIR) pathology zone and assess pharmacodynamics benefits via extracorporeal imaging (theragnostic) at the locoregional pathology.

Keywords: Intermedial HCC, Theragnostic, Subcutaneous liver tumor model, BALB/c2 nude mice, Trans-arterial embolectomy (TAE), Doxorubicin/doxorubicinol, Sorafenib, Trans-arterial Chemo-Embolectomy (TACE), Mass spectroscopy.

Introduction

Primary hepatocellular cancers (HCC) are the most common malignant liver tumors and one of the most lethal malignancies worldwide, marked at 830,000 deaths annually [1–4]. The incidence of HCC in the USA women population was at 2.38 per 100,000 in 2001 rising to 3.9 in 2020, while men have registered at 7.32 to 9.82, respectively. In the USA, HCC is a rare disease where over 42,000 new cases are diagnosed annually and is one of the fastest growing malignancies in terms of cancer-related mortality [5]. Within the pediatric population, HCC is approximately 0.50%-0.60% of all childhood tumors, registered by the FDA as an orphan disease [6-9].

Intermediary HCC (i-HCC) poses special challenges due to presence of multiples tumors at time of diagnosis as well as external metastasis to the liver per se. Hence, options that serve earlier stages of HCC (e.g., liver transplantation, segmental resections) are likely to be denied in favor of chemotherapeutics delivered under guidance (e.g. MRI), aimed for the putative locoregional zone (LRT).

Over the past 2-3 decades, a myriad of treatments' regimens for i-HCC were probed by various putative carriers delivered by TAE (Trans-arterial embolectomy), supplemented by trans-arterial chemo-embolectomy (TACE) combinations yielding modest efficacies termed "Progression free survival", yet rarely reaching "overall survival" (OS) vetted by CRT (controlled randomized trials) [9-12]. With respect to embolectomy, a non-specific, "passive" treatment, introduced to deprive the locoregional tumors of oxygen and essential nutrients thereby sensitizing cancer cells to chemotherapeutics agents. However, due to lack of specificity, normal liver cells and other cellular elements are at risk [13,14]. The most frequent complications following hepatic angio-embolization include hepatic necrosis (15%), abscess formation (7.5%) cholangial damage, and pancreatitis (a severe complication and risk of death). Moreover, embolectomy on its own may not contribute significantly to efficacy without TACE; Likewise, there is no firm evidence to support or refute advantages of either TACE or TAE with respect to efficacy [9-11]. Furthermore, contrast materials and viscous solubilizing fluids (e.g., Lipiodol) confound chemotherapy by perturbation of blood hemodynamics, hemostatic and kidney malfunctions [7,15-19]. Overall, contemporary practices for i-HCC management manifest modest and transient efficacy leaving significant residual unmet burden of disease [19].

Over the past 8 years, Debina diagnostics Inc., (DDI) has been engaged in research aimed at enhancing efficacy and safety of TAE and TACE treatments for i-HCC. Our efforts focus on the development of drug carriers not used to date and abstain from embolectomy, thereby eliminating major, severe safety risks, while preserving and enhancing efficacy [20-22]. Our quest for optimization of carrier's rest on large peer-reviewed reports by leading experts in the nanodiamonds space at large [23-29]. These, continued contributors drew attention to the value of fluorescent diamonds (FD) with respect to high biocompatibility, safety, lending prospect for a theragnostic component based on extra-corporeal NIR imaging as a biomarker for pharmacodynamic consequences.

The scientific community does not seem to be interested in sub-micron FDP-NV-750nm to be developed as a superior carrier of cancer therapeutics for I-HCC [31,32]. The choice of FDP-NV-750nm as a preferred carrier based on vetted biocompatibility of FDP in in vitro (liver cancer cells) and in vivo (rodents, non-human primates) along multiple peer-reviewed publications that strongly support this notion [31-36]. Thus, we characterized FDP-NV-750nm pharmacokinetic, ADME (distribution) and safety biomarkers, organs integrity and functions (e.g., liver functions tests) [34,35]. Furthermore, acute (5 days), subacute (14 days) and prolonged (12 weeks) studies using high doses exposures were sponsored with a CRO known for toxicological services and cancer drug development. Also, the selected carrier, FDP-NV-750nm, was chosen for its robust, stable and durable fluorescence emission in marked contrast to NANO-FDP particles (<1-100nm) that do not generate sufficient emission for whole body imaging by extracorporeal imaging technology. Furthermore, ligation (covalent) and coating with chemotherapeutic agents have been tested in vitro using human liver cancer cells (Hep-G2 and Hep-3B), and confirmed to be up taken and accumulated in liver cancer cell-lines in vitro but spare the nuclei [34]. The

scale and scope of this data are collated in references [31-36]. In summary, our data, along with external, public data, suggest that FDP-NV-750nm is likely to qualify to serve the development of next generation I - HCC treatments.

To affirm this postulation, we pioneered an orthotopic liver xenograft model (mice) and demonstrated strong efficacy in mitigation tumors growth by pre-treatment with FDP-NV-750-DOX-75 [37,38].

The objectives of the present manuscript were set to validate the suitability of FDP-NV-750 nm to serve as an optimized carrier for chemotherapeutics, that are intended to be delivered via trans-arterial procedures, without embolectomy. Specifically: A. Suitability of sub-micron diamonds to carry chemotherapeutic agents via direct tumor injection. B. validate desorption of the 'payload' (e.g., DOX) by direct chemical identity of the carried treatment (DOX) in the tumor; C. verify the pharmacodynamic consequence to DOX desorption, manifested by significant attenuation of tumor growth. D. Lack of severe adverse effects based on animals thriving as a whole and biochemical biomarker such as liver function tests. E. Explore possible synergy with FDP-DOX by association with non-redundant chemotherapeutic (e.g., SOR).

The choice of the chemotherapeutic agent, Doxorubicin, as a primary FDP-bound ligand is based on vast experience with Doxorubicin therapeutic utility in preclinical studies and patients diagnosed with I – HCC [39].Doxorubicin and several anthracyclines hold medical positions as single or adjuvants in multi-regimens of chemotherapeutics combinations. More recently, DOX is delivered by a variety of drug-eluting spheres (DES) and liposome-entrapped Doxorubicin, registered by FDA in 2015 under Doxil®.) [35,39-44]. The latter formulation, Doxil®, has reduced systemic adverse effects but pharmacokinetics disadvantages (e.g., fragility of liposome carrier), systemic organ distribution and liability of aberrant immune-reactions, including complement activation, anaphylactic reaction and immune reactions [42,45]. Hence, we endeavored duplex treatment regimen of non-redundant chemotherapeutic agents such as FDP-NV-DOX+SORAFENIB delivered in tandem.

With respect to the carrier, FDP-NV are known for high biocompatibility, limited systemic distribution and durability that secures slow release of diverse chemotherapeutics [49-54]. FDP-NV-750nm generates very bright and stable NIR emission, which unlike nanodiamonds particles could serve localization of the particles and images of pharmacodynamic consequences post FDP-DOX treatment. Furthermore, we postulate that prolonged residency of deposited particles, and slow desorption of the coating, (e.g., DOX) might prolong the chemotherapeutic impact.

Material and Methods

Diamond Particles acquisition and characterization

FDP-DOX-75 was manufactured by ADAMAS where the Z-average and zeta-potential of FDP-NV and FDP-DOX were assessed by Malvern as previously reported [22-24]. The Z-average and zeta-potential were studied at N=3 as follows: FDP-DOX-75, Z-average at 755+/-3.5 (SD, and standard error of the mean (Sem) of 2.07 +/- 0.22 mV. The zeta potential of FDP-DOX-75 was minus 21.2 +/- 0.11 mV SD (or 0.11 Sem). Since FDP-DOX-75 was suspended in 3 % BSA (bovine serum albumin), a negatively charged protein, the coated particles retained a negative (21mV) post-coating, as compared to a positive surface charge when particles are suspended in PBS. suspension in PBS) FDP-NV-750nm (FDP-NV) were functionalized at the manufacturer (Raleigh, NC, USA). Coating ligands of protonated chemical moieties (e.g., primary nitrogen) onto the negative charge of FDP-750 surface. Doxorubicin was purchased from MedKoo Biosciences, (Morrisville, NC, USA). The coating process and desorption profile (conducted by the supplier) have been detailed in our recent publications The FDP-DOX-75 μg/mg, was delivered in autoclaved Eppendorf vials at 0.1 mg/mL of deionized water. FDP-DOX were provided in various DOX coatings up to FDP-DOX-75 μg/mg particles. Particles were sterilized at the manufacturer and suspended in sterile deionized water in sterile plastic Eppendorf tubes. Z-average and surface charges/potential of FDP-NV-750 nm before and after coating with doxorubicin.

Dispersion of particles by sonication prior to infusion to animals

Due to the innate tendency of FDP-NV-750nm (FDP-NV) for agglomeration in electrolyte solutions (normal saline, PBS pH=7.4) all suspensions of particles were subjected to vortex mixing followed by sonication. To facilitate dispersion, BSA at 3% was added to PBS pH=7.4 and the suspension was subjected to high vortex stirring for 3 min followed by sonication in a water bath for 10–15 minutes using a Digital ultrasonic cleaner machine (Kq-50TDB, Kunshan Ultrasonic Instrument Co Ltd, Jiangsu, China) at 150 W and a frequency of 80 kHz while maintaining water temperature in the range of 20–25°C; an example of particles dispersion after sonication is provided in reference [35,39].

Human liver cancer-cells: acquisition and application.

Hep-3B-luc human liver cancer cells were obtained from WuXiAppTec (Shanghai, China). Cells were kept in medium supplemented with 10% fetal bovine serum at 37°C with 5% CO_2 in air. Hep-3B-luc tumor cells were sub-cultured twice weekly, during the exponential growth phase, and harvested for tumor inoculation at $3x10^6$ cells per mouse. Cells were inoculated into the right auxiliary subcutaneous space under adequate anesthesia. Tumors growths were monitored by palpation and a caliper device. Periodic Bioluminescence was tracked following intravenous injection of luciferin suspension.

In vivo mice studies

BALB/C2 'nude' mice acquisition, husbandry and auxiliary subcutaneous Hep-3B-luc tumor model

Female BALB/c 'nude' mice (20–22 g, 6–8 weeks old) were purchased from Beijing Vital River Laboratory Animal Co Ltd for use at WuXiAppTec facilities (Shanghai, China). All *in vivo* protocols exercised at WuXiAppTec (shanghai, China) and performed under accredited procedures as per

Chinese Regulatory Agency and according to IACUC, are in line with US FDA guidelines. Subcutaneous liver cancer model (Hep3B-luc) was established by injecting $3x10^6$ Hep-3B-luc cells suspended in twenty µL Matrigel (1:1/w: w) into the axillary space of BALB/c "nude" mice, under proper anesthesia. Luciferin challenges by intravenous injections elicted robust images for bioluminescence monitored by IVIS (in Vivo Imaging System) performed as described in our previous report [39].

Luciferin induced bioluminescence of Hep-3B-luc tumors in BALB/c "NUDE" mice

BALB/c 'Nude' mice inoculated with Hep-3B-luc cells were administered intravenously with luciferin suspension via tail vein at a dose of 150 mg/kg. Five to ten minutes after injection of luciferin, the animals were lightly anesthetized by inhalation of 2% isoflurane in air. Upon proper anesthetic state, mice were transferred into IVIS imaging chamber for bioluminescence measurements using the Lumina III (PerkinElmer, Inc., Waltham, USA) imaging system. Bioluminescence signals were collected 15 min after injection of luciferin (at peak) was as the maximum value.

Ex vivo monitoring of tumor bioluminescence and FDP NIR fluorescence in DOX-treated mice for tumor imaging.

Injections of FDP-NV-750 nm and FDP-750-DOX into isolated tumors and ancillary organs was measured by IVIS Lumina III (PerkinElmer, Inc., California USA) using Ex/Em setting at 580 nm and 720 nm respectively, with auto-exposure setting time and 'binning' set at 4. All *ex vivo* images of organs were performed following dissection at the termination day of the protocol. The whole-body perfusion of the mice was performed under deep anesthesia by cardiac puncture using sterile normal saline.

Euthanasia of mice by pre-determined unbiased thriving criterion

Euthanasia was induced in accordance with WuXi humane guidelines to avoid painful or stressful conditions. Mice were placed in a chamber ventilated with at least 95% CO_2 and maintained at 2.7 L/min to 6.3 L/min throughout. At the point of complete cessation of motor activity, breathing, and complete unconsciousness, a cardiac puncture was performed to commence organs perfusion with 10 mL of sterile, isotonic saline and remove residual blood in the vasculature of the animal. Organs were preserved in 4.5% buffered formaldehyde.

Monitoring liver biomarkers in FDP-DOX treated mice.

Arterial blood was withdrawn by cardiac puncture under proper anesthesia (5% isoflurane) and collected into anti-coagulant-containing syringes (EDTA). Liver functions tests (LFT) and normal hematological variables (data not shown) were processed using standard clinical biochemistry methods.

Doxorubicin/Doxorubicinol extraction from tumors exposed to FDP-DOX

Total Doxorubicin was extracted from whole tumors immediately after euthanasia. FDP-DOX treated mice were analyzed using ultra high-performance liquid chromatography coupled to tandem mass spectrometry (UPLC-MS/MS). Tumor tissue was homogenized with 9 volumes (w:v) of homogenizing solution (1*PBS buffer). An aliquot of 60 µL was taken from the calibration standard for quality control. A single blank, and double blank sample were added to 1.5 mL tube, respectively. All samples were spiked with equal volume of 1% HCl in water and mixed well. All samples were incubated at 37°C for 7h. Each sample (except the double blank) was quenched with 300 µL of 100 ng/mL Labetalol & amp; tolbutamide & amp; Verapamil & amp, dexamethasone & amp; glyburide & amp; Celecoxib in MeOH with 1% HCl respectively. Double blank sample was quenched with 300 µL of MeOH with 1% HCl), followed by vortex mixing over 15 sec and centrifuged for 15 min at 12000 × g, at 4°C. An aliquot of 50 µL supernatant was transferred to a new 96-well plate and centrifuged for 5 min at 3220 × g, 4°C. Then, the supernatant was directly injected for LC-MS/MS analysis.

LC-MS/MS was performed by ACQUITY UPLC System with an ACQUITYUPLC HSS T3 1.8 µm 2.1 × 50 mm column and a Triple Quad 6500 plus mass spectrometer. Retention time, plotting of the chromatograms and peak area integrations and calculations were carried out by using Multi-Quant (Sciex, Version 3.0.3, Framingham, Massachusetts, USA).

Analytical methods

Free Doxorubicin, total Doxorubicin and Doxorubicinol extracted from tumors ex vivo was analyzed using ultra high-performance liquid chromatography coupled to tandem mass spectrometry (UPLC-MS/MS). The tissue was homogenized with 9 volumes (W:V) of homogenizing solution (1*PBS buffer). An aliquot of unknown sample, calibration standard, quality control, single blank, and double blank sample were added to the 1.5 mL tube, respectively. Each sample (except the double blank) was quenched with precipitant containing internal standards respectively (Labetalol & tolbutamide & Verapamil & dexamethasone & glyburide & Celecoxib). For free Doxorubicin, 40 µL sample was quenched with 200 µL of ACN; For total Doxorubicin, 60 µL sample was added with equal volume of 1% HCl in water, mixed well, incubated at 37°C for 7h, then quenched with 300 µL of MeOH with 1% HCl.

For Doxorubicinol, 100 µL sample was quenched with 400 µL MeOH; Double blank sample was quenched with precipitant without internal standards.

The mixture was vortex-mixed (at least 15 s) and centrifuged for 15 min at 12000 × g, 4 °C. An aliquot of 50 µL supernatant was transferred to 96-well plate and centrifuged for 5 min at 3220 × g, 4 °C, then the supernatant was directly injected for LC-MS/MS analysis. The whole process for free Doxorubicin was done on wet ice.

LC-MS/MS was performed on a ACQUITY UPLC System with a ACQUITY UPLC HSS T3 1.8 µm 2.1 × 50 mm column and a Triple Quad 6500 plus mass spectrometer. Retention time, plotting of the chromatograms and peak area integrations

and calculations were carried out by using Multi-Quant (Sciex, Version 3.0.3, Framingham, Massachusetts, USA).

Extraction and assay of total doxorubicinol

Doxorubicinol was analyzed using ultra high-performance liquid chromatography coupled to tandem mass spectrometry (UPLC-MS/MS). Tissue was homogenized with 9 volumes (w:v) of homogenizing solution (1*PBS buffer). An aliquot of 100 µL from the unknown sample, calibration standard, single blank, and double blank sample were added to the 1.5 mL tube respectively. Each sample (except the double blank) was quenched with 400 µL of 100 ng/mL Labetalol & amp; tolbutamide & amp; Verapamil & amp; dexamethasone & glyburide & Celecoxib in MeOH (double blank sample was quenched with 400 µL of MeOH), and then the mixture was vortex-mixed well (at least 15 sec) and centrifuged for 15 min at 12000 × g, 4 °C. An aliquot of 50 µL supernatant was transferred to the 96-well plate and centrifuged for 5 min at 3220 × g, 4 °C, then the supernatant was directly injected for LC-MS/MS analysis.

LC-MS/MS was performed by using an ACQUITY UPLC System with ACQUITY UPLC HSS T3 1.8 µm 2.1 × 50 mm column and a Triple Quad 6500 plus mass spectrometer. Retention time, plotting of the chromatograms and peak area integrations and calculations were carried out by using MultiQuant (Sciex, Version 3.0.3, Framingham, Massachusetts, USA).

Histology, histochemistry and fluorescence microscopy

Preparation of slices: Paraffin preserved blocks were - sectioned at 4-5 µm by a manual rotary microtome (Histoscore 'Multicut', Leica GmbH, Wentzler, Germany).

H&E and DAPI staining: Slices were exposed to 60°C for 1 hour for complete dewaxing following which, the specimens were transferred to Tissue-Tek Prisma® Plus auto stain (Sakura Fintech, Torrance, CA, USA) Stained slides were scanned with panoramic digital slide scanners (panoramic SCAN, 3DHISTECH Kit, Budapest, Hungary). An expert of liver pathologist evaluated high-resolution images.

AFP (Alpha-Feto protein) immunohistochemistry: Slides were scanned with panoramic digital slide scanners (panoramic Scan, 3D HISTECH Kft, Budapest, Hungary) under filters. High-resolution imaging for whole sections was generated and analyzed. For additional technical details, see references [21-23].

Liver Phagocytic cells, CD68+ immunohistochemistry: CD68 (macrosialin) is a heavily glycosylated transmembrane protein that is commonly used as a marker for monocytes and macrophages. We used CD68+ as a biomarker to locate macrophages in this study. Slides were exposed to 60°C for an hour to dewax and then transferred to Bond RX auto Stainer (Leica GmbH, Wetzlar, Deutschland) for IHC staining. The primary antibody used for IHC is anti-CD68+ (CST #97778). Macrosialin, a macrophage-restricted membrane sialoprotein differentially glycosylated in response to inflammatory stimuli [47].

Pharmacokinetics and Pharmacodynamic of Sorafenib in in vitro system of Hep-3B-luc liver cancer using Alamar Blue as indicator of cell viability

Cells were seeded on the 96-well plate at density 1 x 10 4 per well in complete growing medium (EMEM containing 10% FBS). Cells were allowed to attach overnight at 37°C in 5% CO_2 atmosphere, and medium was exchanged serum-free in volume 150 ml per well. Cells were incubated at 37°C in 5% CO_2 atmosphere for 24, 48 and 72 hours. Medium was removed and cells were washed once with 200 ml of FBS-free DMEM. Alamar Blue (Thermo-Fisher) was diluted 1:10 with FBS-free medium and added to the wells in volume 100 ml. Plates were incubated for 1 hour at 37°C in 5% CO_2 atmosphere and read using florescence microplate reader (Tecan) with 540 nm Ex and 590 Em wave lengths.

Imaging technology

All images were scanned at 40x magnification (panoramic SCAN, 3DHISTECH Kft, Budapest, Hungary), Hematoxylin and Eosin (H&E) images were generated at bright field and fluorescence images were generated with DAPI (Ex/Em= 377/447) for nuclei imaging, SpGr-B (Ex / Em=494/527), while DOX and SpRed (Ex/Em=586/628) for FDP-NV. All images were obtained with Case Viewer V2.4 (3DHISTECH Kft, Budapest, Hungary). All H&E images were analyzed using the HALOTM platform (Indica Labs, Albuquerque, NM, USA).

Tumor area evaluation

The tumor area distinguished by H&E staining was easily differentiated from liver cells zones (using the Annotations model in HALO). The tumor area was calculated using software, which included, in addition to tumor cells, hollow zones, necrosis, and stroma.

Tumor cell evaluation was performed using hollow, necrosis, and stromal classifier tumor cells based on staining differences (with Classifiers model in HALO). The tumor cell area was calculated by software, for tumor cells only.

Tumor cell counts: Cells were identified by nuclei using the Cytonuclear model in HALO and the model was run on the tumor cell area obtained above; tumor cell counts were calculated by software. Data were imported into GraphPad Prism (GraphPad Software, San Diego, CA, USA) from which the bar graph was generated including error lines that represent standard error of the mean (Sem) based on n=5 for each of the three variables in (***) $P < 0.001$ calculated by

Alfa-Fetoprotein and immunohistochemistry

Alfa-Fetoprotein (AFT) is an oncofetal liver antigen that is normally produced transiently by the fetal liver, but ceases expression in adults when the immune system is fully developed [39]. AFP is commonly used as a biomarker to monitor treatment outcome in patients with HCC [44,45]. Because Hep-3B-luc are known to express AFT, we used this protein as a biomarker to differentiate tumor cells from hepatocytes, immune cells (macrophages and other cells of the tumor microenvironment.

Liver slices 4-µm-thick were sectioned by Leica RM2235 Manual Rotary Microtome (Leica Microsystems GmbH,

Germany), then deparaffinized/rehydrated by sequential washing (Xylene, ~100–75% Ethanol and PBS). After antigen retrieval by the microwave heating in EDTA buffer (MVS-0098, MXB Biotechnologies, Foochow, China) and peroxidase quenching in 3% hydrogen peroxide for 5 min, the slides were blocked by blocking buffer (SP KIT-B2, MXB Biotechnologies, Foochow, China) and stained using primary Anti-alpha 1 fetoprotein antibody (Anti-AFP, #284388, Abcam) at 1:50 dilution in antibody dilution buffer (#AR9352, Leica) overnight at 4 °C using the Opal 7-Color Automation IHC Kit 50 (NEL821001KT, PerkinElmer, USA). Subsequently, the DAPI stained slides were mounted with Prolong Diamond Antifade mounting (P36961, Invitrogen) and scanned with Aperio Versa 8 (Leica Microsystems GmbH, Germany).

Data presentation, analysis, and statistics

Data are presented as mean ±1 SD or standard error of the mean (SEM) as indicated in the figure legends. Statistical analyses were performed by ANOVA, using SigmaPlot software (SigmaPlot® 12 SPSS, Systat Software Inc., San Jose, CA, USA). Statistical significance was established at $P< 0.05$. Plots were prepared using SigmaPlot software. For the nonlinear regression dynamic fitting plot, the standard four-parameter logistic curve was drafted using SigmaPlot software. A mixed model ANOVA on log transformed luminescence was performed for the analysis of tumor bioluminescence assessed by whole body luminescence. Treatment and time were analyzed as fixed effects, and interaction was also included. Animals were considered a random effect nested within treatment and analyzed using the REML method to account for the repeated measures. Three samples registered a luminescence far below other samples and were excluded from the analysis. The residuals appeared normal and uncorrelated, with Shapiro–Wilk and Anderson–Darling $p > 0.3$. ANOVA and all fixed effects were significant with $P <0.0001$. Test slices of the interaction were used to assess the time dependence of the treatment and control groups. For specific time point comparisons, Tukey HSD post hoc was used with $\alpha = 0.01$.

Results

Effect of FDP-DOX injected directly into subcutaneous Hep-3B-luc tumors on growth kinetics throughout 52 days

Table 1 provides general, high-level information on the experimental groups that were studied, suspensions prepared for injections and scheduled for injections. Tables 2 presents the systematic protocol of treatments and measurements for all groups studied. Table 3 presents dosing information and timelines for Sorafenib. Figures 1,2,3,4, and 5 display the kinetics of tumor growth for each of the treatments up to 52 days. Figure 3 and 4 analyzed the kinetic of tumors' growth subjected to FDP-DOX Vs the 2 controls (vehicle and bare FDP-NV). A statistically significant difference and power (N) between treated (FDP-DOX) and controls is provided by the insert in each group figure. Figure 3 informs FDP-DOX effect on rate change by direct volume measurement and by calculation of percent change. The 2 control groups displayed tight similarity, reaching significantly larger volume over that of FDP-DOX treated group. This data was also analyzed by a percentage change of tumors growth between treated (FDP-DOX) and fits the direct volume measurements. It is important to note that by day 52, the FDP-DOX treated group exceeded 53% reduction in its volume over the joint control groups.

Effects of FDP-DOX injected directly into subcutaneous tumors on bioluminescence of Hep-3B-luc cells measured by fluorescein emitted bio-fluorescence

Hep-3B-luc cells implanted subcutaneously are featured with luciferase genes. These cells express luciferase, an enzyme that activates fluorescence upon electro-magnetic radiation. Therefore, upon systemic injection of the luciferin, fluorescence could serve as a proxy to the overall mass of viable Hep-3B-luc. Figure 4 presents the effects of FDP-DOX on viable Hep-3B-luc exposed to luciferin. Tumors of the control groups preserve their mass of viable Hep-3B-luc

Days	Treatment			Measurement		
	Vehicle, i.t.	FDP-NV, i.t.	FDP-DOX, i.t.			
17	20µL	20µg	20µg			
18						
20	40µL	120µg	120µg			
24	60µL	180µg	180µg			
27	60µL	180µg	180µg			
31	70µL	210µg	210µg			
34	80µL	240µg	240µg			
35						
38						
39	80µL		240µg			
40						
41	80µL		240µg			
43	80µL		240µg			
44						
45						
49						
52						

	Tumor Volume
	Bioluminescence
	Fluorescence

Table 1: Summarizes schedule of treatments with FDP-DOX, Vs 2 different controls: vehicle and FDP-NV "naiive" as compared to FDP-DOX. The timing of injections (day) is displayed in the left column; the dose (volume, µL) were compared to control group and FDP-DOX. The latter treatment was delivered in a suspension of PBS containing 3% BSA and injected directed into tumor after brisk vortex.

Days	Treatment					Measurement		
	Vehicle, i.t.	FDP-DOX, i.t.	Sorafenib, i.t.	FDP-DOX, i.t. + Sorafenib, i.t.				
17	20µL	20µg		20µg				
18			0.3µM		0.3µM			
20	40µL	120µg		120µg	0.6µM			
24	60µL	180µg		180µg	1.2µM			
27	60µL	180µg		180µg	4.8µM			
31	70µL	210µg		210µg	0.6µM			
34	80µL	240µg		240µg				
35			30mg/Kg		30mg/Kg			
38								
39		240µg		240µg				
40			72mg/Kg		72mg/Kg			
41								
43				240µg				
44								

Table 2: This table provides the same parameters but in an extended elaboration of the protocol and one difference: sorafenib treatments alone was added and the combination of FDP-DOX and sorafenib injected in tandem at the doses and times (days) listed in column 1.

Tumors were established by subcutaneously injecting Hep3B-Luc cells into the flank of female Balb/c2 nude mice. The date of injection was noted as Day 0, and tumor size was measured periodically in two dimensions using a caliper. On Day 17, the tumor bearing animals were randomized by tumor volume and the treatment started. Table 2), described the same parameters of FDP-DOX and FDP-DOX combined with Sorafenib injections in tandem to FDP-DOX (via separate injections spaced 24-48 hours) following FDP-DOX treatment. Injection volume and amount of the carrier are detailed in table 3, and the date of measurement were marked as color blocks (violet, for tumor volume; blue, for bioluminescence and pink for fluorescence). Thriving, assessed by whole body weight, (pink box) with 20% reduction used as trigger for euthanasia as per regulatory requirement.

Date	D18	D20	D24	D27	D31	D35	D40
Volume	3% Tumor volume					50µL	60µL
Dosage	0.3µM	0.6µM	1.2µM	4.8µM	19.2µM	30mg/kg	72mg/kg
Concentration	0.05µg/µL	0.09µg/µL	0.19µg/µL	0.74µg/µL	2.97µg/µL	12µg/µL	24µg/µL
Dosage: start from 0.3µM in tumor, and duplicate in each next injection. The final 2 doses were 30 and 72mg/kg.							

Table 3: Provides parameters of sorafenib (SOR) injection as a single chemotherapeutic commencing on day 18 post inoculation and followed up to day 40. SOR suspension was delivered in suspension.

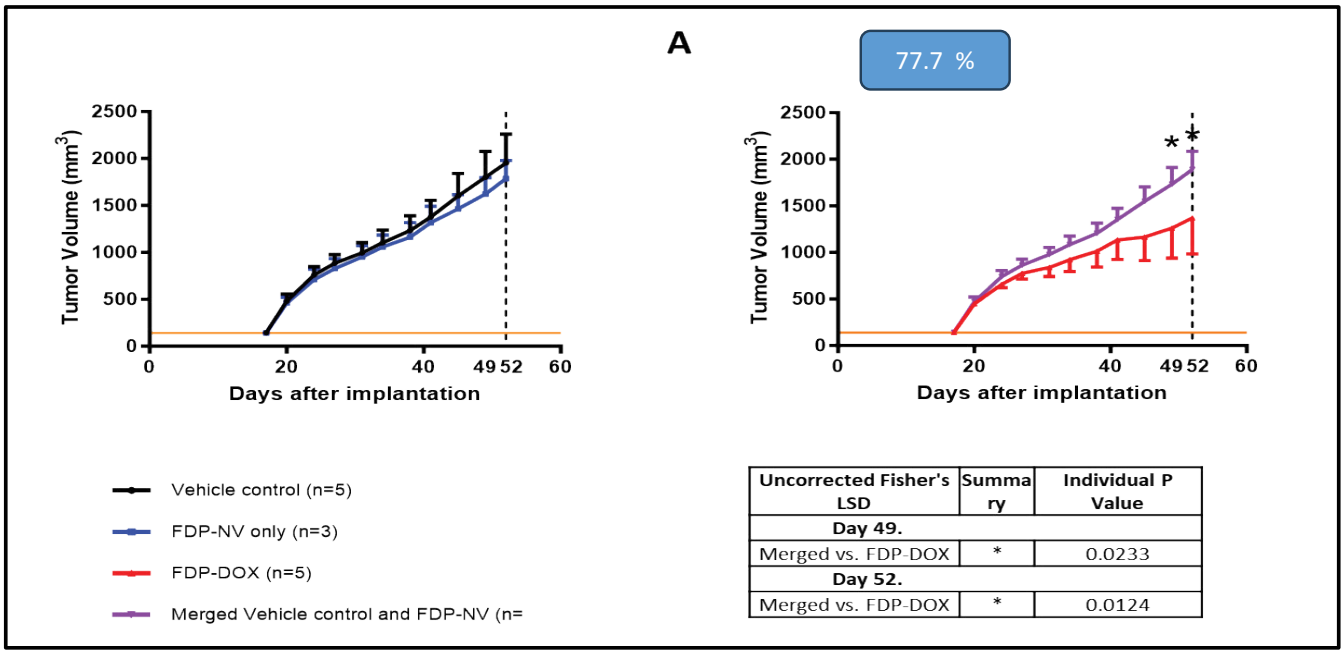

Uncorrected Fisher's LSD	Summary	Individual P Value
Day 49.		
Merged vs. FDP-DOX	*	0.0233
Day 52.		
Merged vs. FDP-DOX	*	0.0124

Figure 1: Effect of FDP-DOX on Hep-3B-luc tumors growth in auxiliary space of BALB/c nude mice. Asterisks in the table insert provide statistical significance for the respective p-values listed in the table.
Data presents changes in tumors' volume progression calculated by caliper methods. No statistical differences were established between the 2 controls. FDP-DOX treated mice (figure 1) present modest growth retardation presented in the box of 23% of the controls. The calculation of the differential between treated and controls was done by calculating the ratio of top growth of the treated group by top growth of the merged controls and multiplied by 100%.

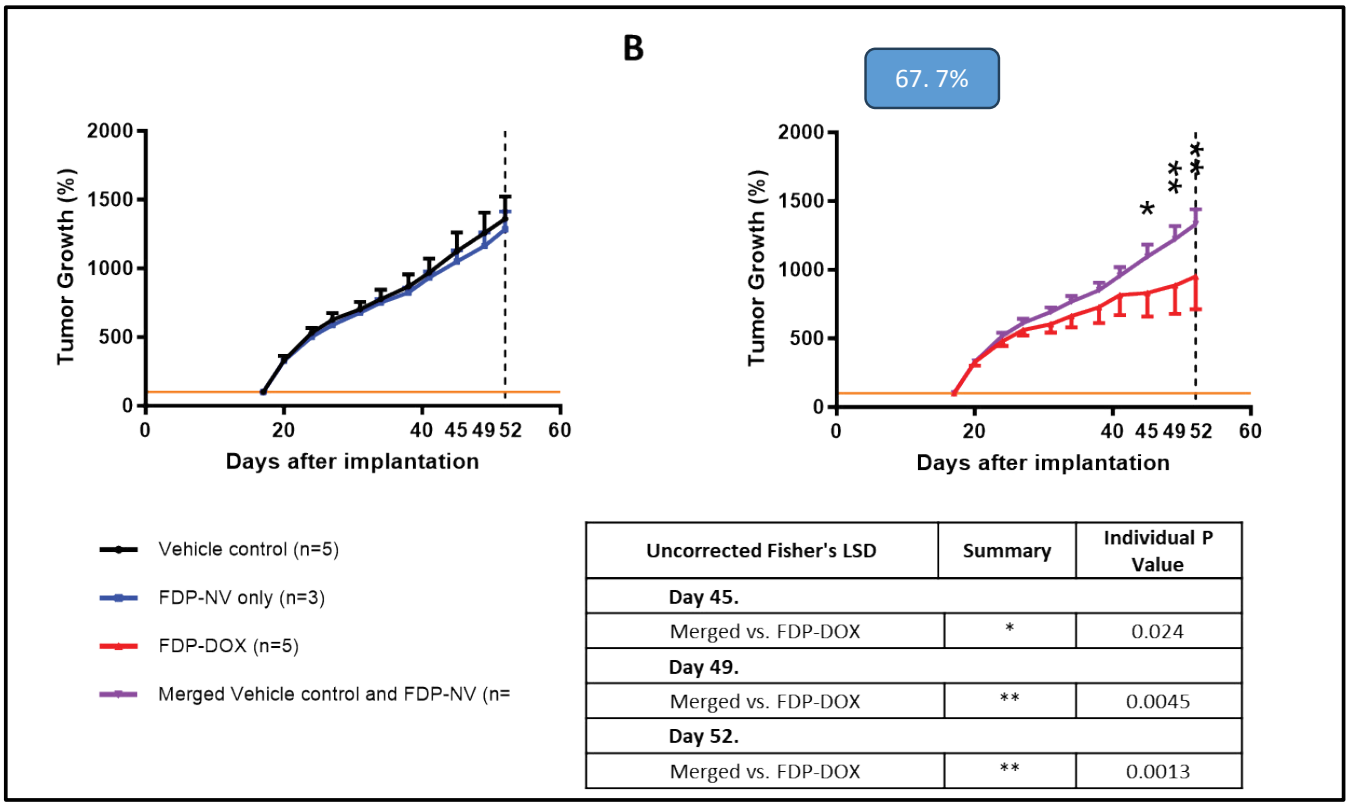

Uncorrected Fisher's LSD	Summary	Individual P Value
Day 45.		
Merged vs. FDP-DOX	*	0.024
Day 49.		
Merged vs. FDP-DOX	**	0.0045
Day 52.		
Merged vs. FDP-DOX	**	0.0013

Figure 2: Figure 2 follows the design of figure 1 for validation. Tumor growth of the FDP-DOX treated group displays 23 % of the merged control calculated as described vide supra. expressed as a percentage of changes of tumor volume throughout the duration of growth. Merged control line (pink) represents summation of the 2 controls (black line, PBS) and FDP-DOX (blue line) (FDP free of DOX). The percentage of reduction of tumor volume for day 52 between merged control and FDP-DOX treated was somewhat lower values- 27.5%.

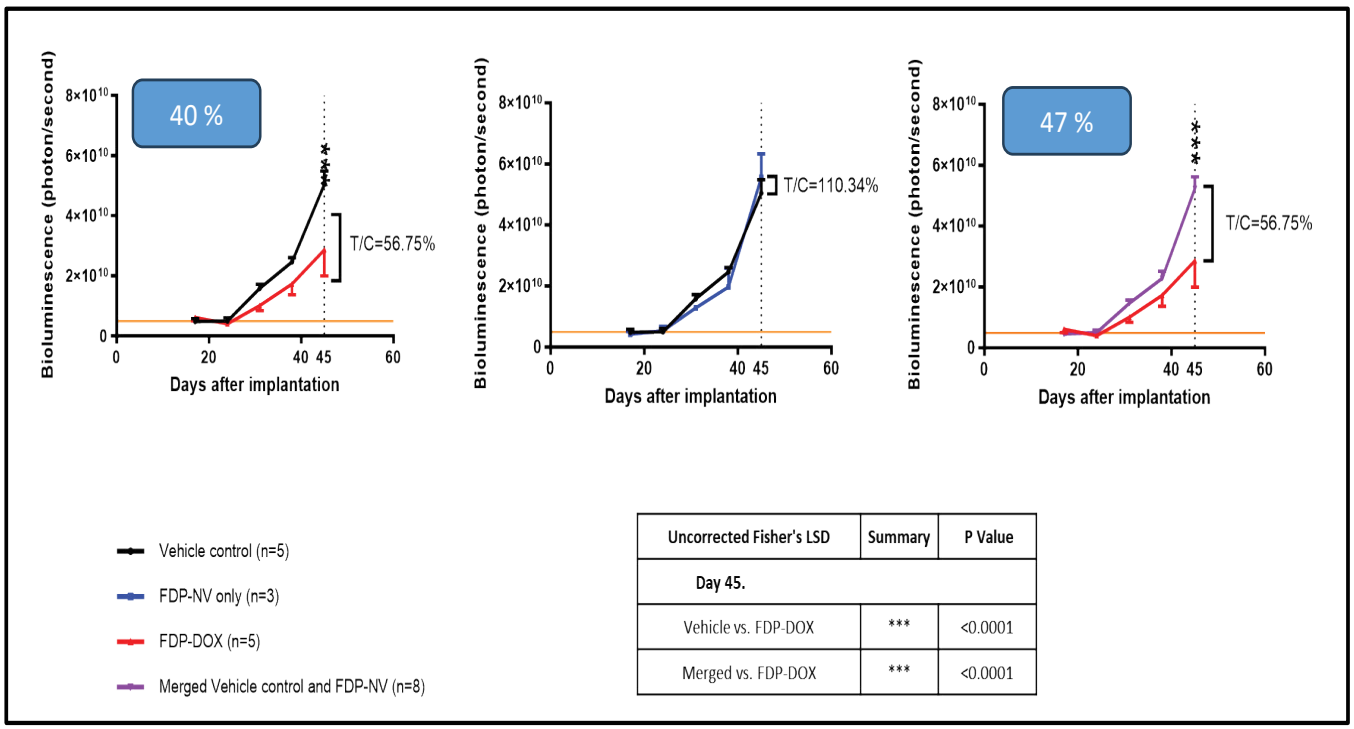

Uncorrected Fisher's LSD	Summary	P Value
Day 45.		
Vehicle vs. FDP-DOX	***	<0.0001
Merged vs. FDP-DOX	***	<0.0001

Figure 3: presents the effect of FDP-DOX on tumor biolumnescence of the Hep-3B-luc monitored by luciferin injection.The differential bioluminescence between the FDP-DOX and vehicle contol or the merged control Vs the FDP-DOX treatment are provided vide infra. Statistical analysis indicate similar differential whether vehicle control or merged control.

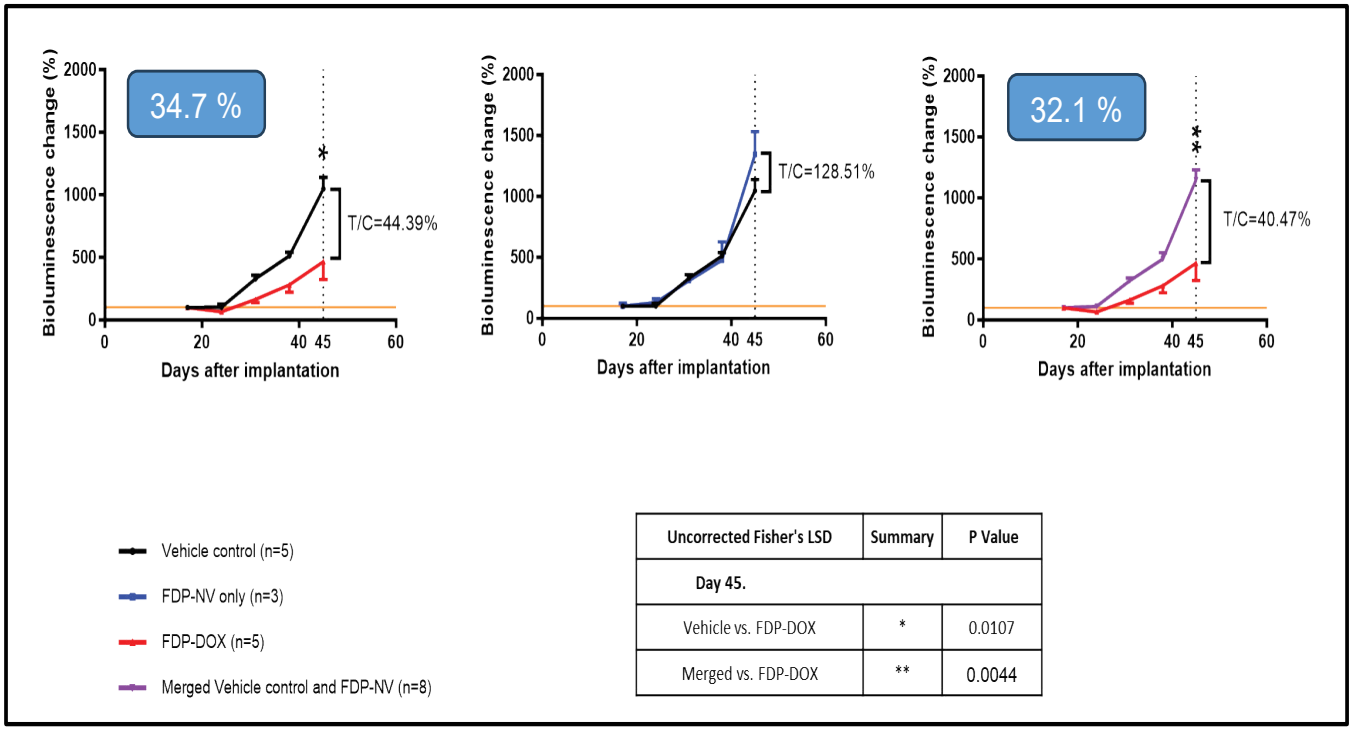

Uncorrected Fisher's LSD	Summary	P Value
Day 45.		
Vehicle vs. FDP-DOX	*	0.0107
Merged vs. FDP-DOX	**	0.0044

Figure 4: Figure 4 tested the efficacy of ADP-DOX in attenuation of tumor growth measured by bioluminescence of hep-3B-luc cancer cells charged with luciferin. The impact of FDP-DOX is virtually the same whether Vs vehicle control or merged control. The 2 controls display a minor difference but not a statistical significance. The power of each group is displayed in color coded line left to the insert.

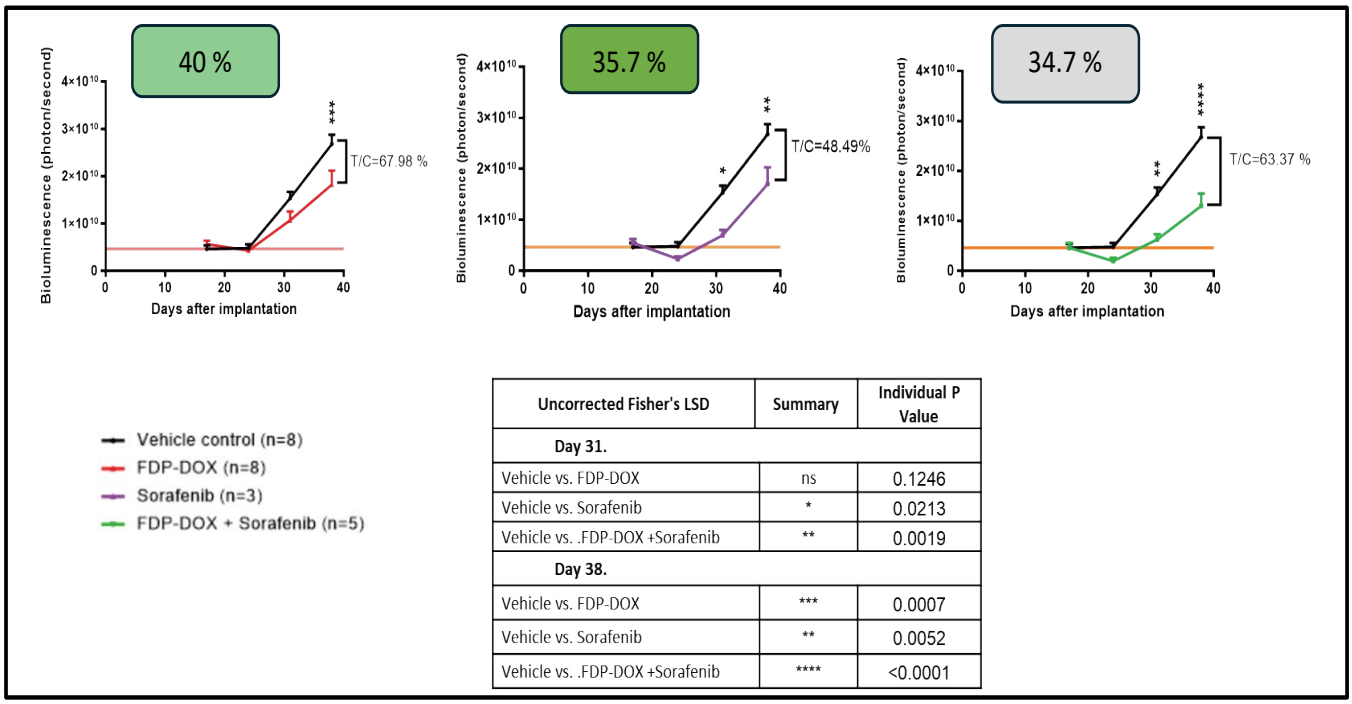

Uncorrected Fisher's LSD	Summary	Individual P Value
Day 31.		
Vehicle vs. FDP-DOX	ns	0.1246
Vehicle vs. Sorafenib	*	0.0213
Vehicle vs. .FDP-DOX +Sorafenib	**	0.0019
Day 38.		
Vehicle vs. FDP-DOX	***	0.0007
Vehicle vs. Sorafenib	**	0.0052
Vehicle vs. .FDP-DOX +Sorafenib	****	<0.0001

Figure 5: Effect of FDP-DOX on tumor growth in experimental subcutaneous BALB/c nude mice carrying Hep-3B-luc (human hepatocellular carcinoma) inoculated into an axial space of immune impaired mice. Tumor growth is presented as a percent change from baseline bioluminescence used as a proxy" for tumor growth. All treatments were compared to vehicle control (black line, table insert) where 3 mice have been collated. Percent change from first bioluminescence (base line) and three repeats thereafter monitored at N=3 as illustrated by color coded lines. Statistical differences between treated and controls are presented in the inserted table on days 31 and day 38; the latter include statistical significance at powers listed for each group. Bioluminescence was monitored by IVIS as described in the method section. Asterisks displayed in the inserted table represent statistical significance for each of the treated groups. The percentage of biofluorescence for day 38 between control and FDP-DOX reached 53.8% at p<0.0052-0.0001.

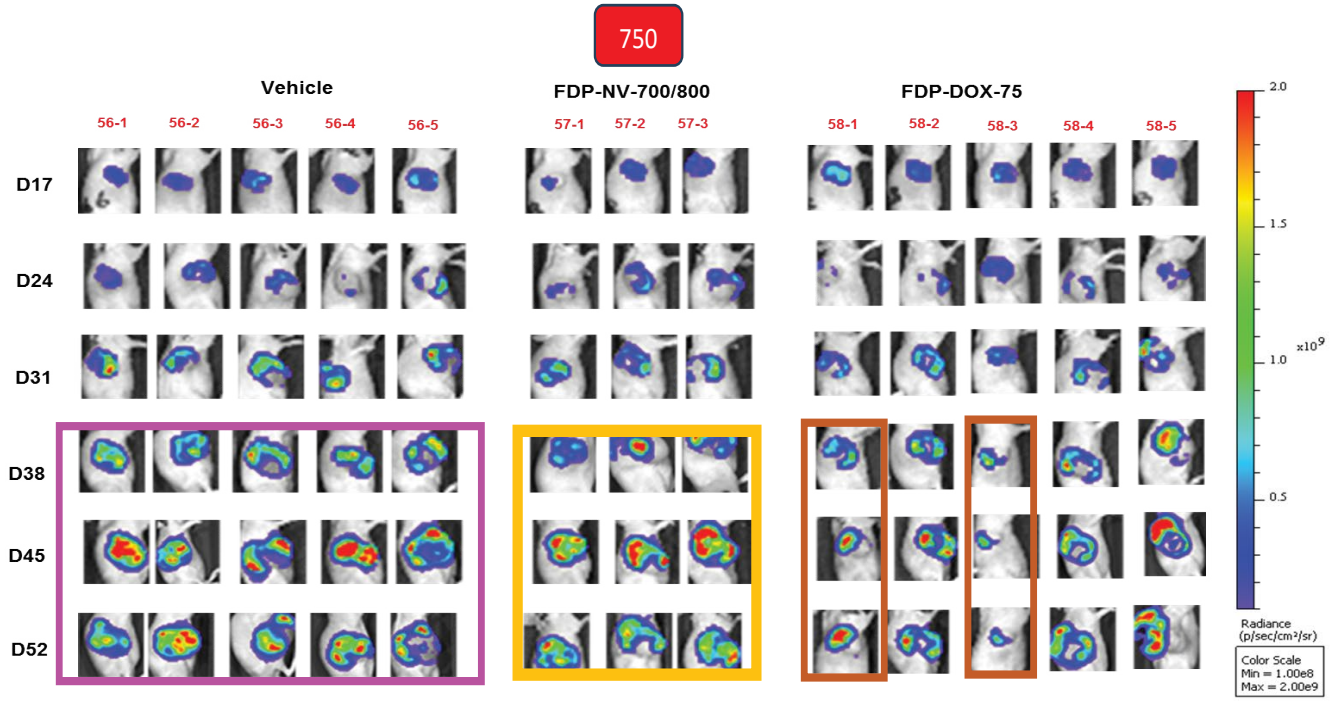

Figure 6: Whole body images by IVIS which illustrate the tumors growth in the three groups: vehicle controls, FDP-NV-750 (controls), and FDP-DOX treated of tumors. Vehicle controls exhibit robust and steady growth of tumors (pink box,) the FDP-NV naïve (yellow box) and FDP-DOX treated (black box). The pink and yellow boxes illustrate the expected growth pattern of the Hep-3B-luc tumors. The FDP-DOX (black box) provides clear visible retardation of tumors growth albeit in various extents. In particular, tumors in the black box, and in particular tumor #58-1 and more so, #58-3, (shown in brown frames) present complete arrest of tumor growth. which commenced on day 38 (of the designated D 52).

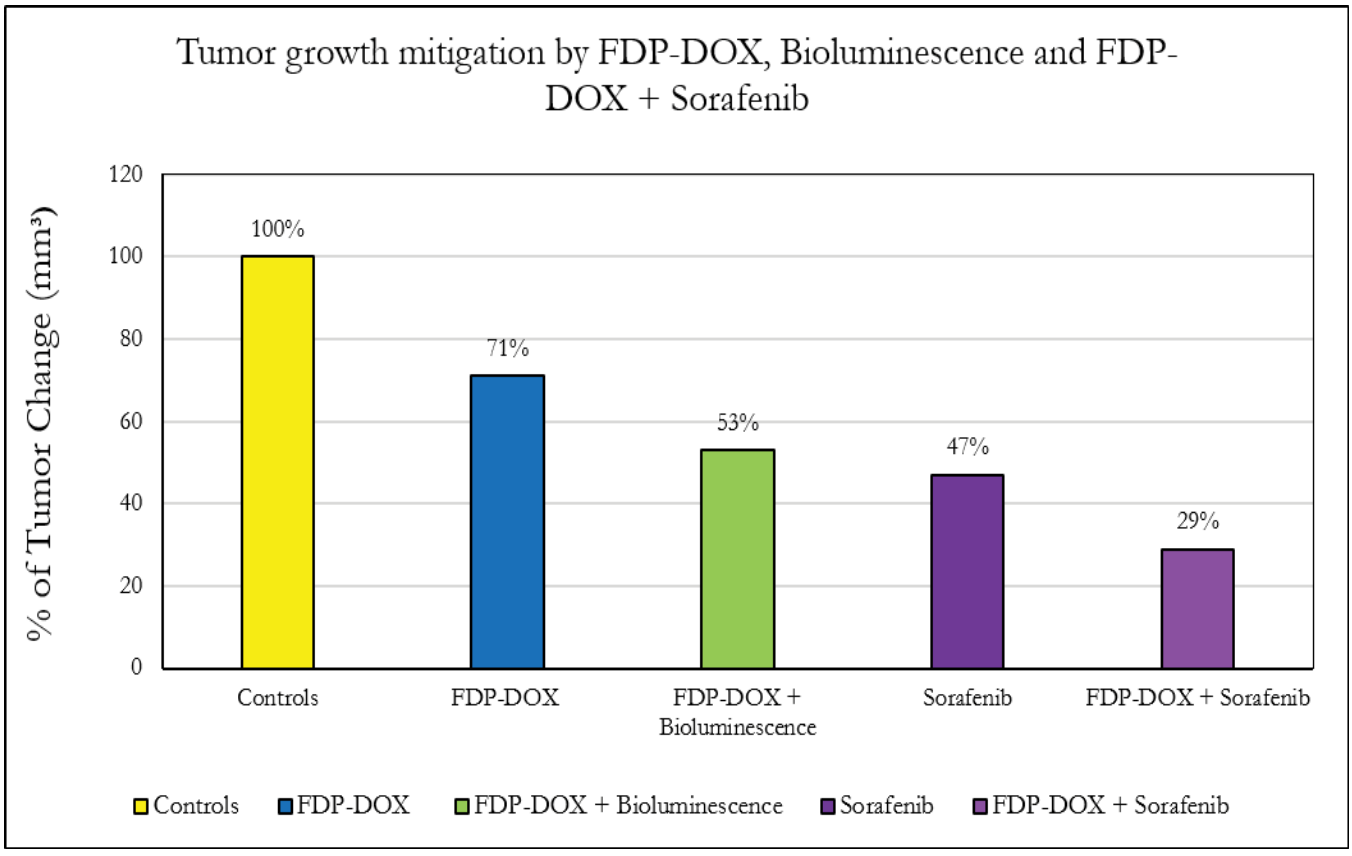

Figure 7: representation of efficacy of each treatment with respect to the biomarkers of tumor percent of cells proliferation and/or bioluminescence of Hep-3B-luc cancer cells.
TV= tumor volume; BL=bioluminescence.

cells yet over 53% of the emission is lost in FDP-DOX treated mice. Thus, the efficacy of FDP-DOX in reducing mass of tumors' cells serves an independent biomarker of treatment efficacy. Statistical analysis provides high significance as presented in the insert of figure 4.

Whole body imaging of mice inoculated by Hep3B-luc to afford direct visual inspection of tumor growth kinetics over 44 days (Figure 6).

Three groups have been studied:1) vehicle control group (N=5), 2) FDP-NV-750 (N=3, no DOX coated) and FDP-DOX treated (N=5). Control group displayed steady growth of tumors and so also FDP-NV-750 (barren). FDP-DOX treated tumors show more diversity with regard to size of fluorescence; the control group display strong fluorescence and tumor perimeter and so also the naïve FDP-NV-750; In marked contrast, FDP-DOX treated tumors were invariably smaller: mice number 1 and 3 show complete arrest of tumors' progression already at day 31 and further on to almost growth arrested. Mice 2 and 4 are also visually smaller up to day 52. Only one tumor, number # 4, reached a size comparable to the control (see framed illustration in figure 6; the reason for this outstanding data has not been investigated as it is nor core issue to the study objectives. Verification of the presence of FDP-NV-750 injected into the tumors of mice inoculated with Hep-3B-luc and injected FDP-DOX, were needed to ensure that mice that did not get the injection do not display NIR within the tumor and therefore qualify for exclusion while NIR emission from a tumor serves as an unequivocal inclusion to the group injected FDP-DOX. Yet all mice bearing tumors that were injected with the FDP-DOX could be verified by NIR emission and qualify as an inclusion and attesting to successful injection of FDP-DOX. It is of interest to note that mouse number 3 in the FDP-DOX treated group (see purple box in figure 7) displays exceptional strong NIR emission suggesting possible overdose; this is in line with the observation that mouse 3 in FDP-DOX group has shown early impact of the treatment and virtually complete annihilation of the tumor by day 52.

Detection of doxorubicin and its metabolite, doxorubicinol, in tumors subjected to FDP-DOX injections

Prolog: Identification of DOX in tumors following FDP-NV-DOX direct to tumor injection is an essential part for probing desorption of the chemotherapeutics into the tumor; It virtually serves as a "gate" step for further investment in the development of the program. Therefore, we have contracted with an experienced and reputable CRO (Contract Research Organization) known for conducting sophisticated chemistry analyses. Table 4 provides detailed actions for analytical procedures, building standards and deploying adequate assay: liquid chromatography and Mass spectroscopy. Figure 8 provides examples for isolation and analysis of doxorubicin and doxorubicinol directly from the tumors. Presented in quantitative results for the compounds of interest. We ask that this information remains in the manuscript text since no known comparable report could be found in the public domain. Figures 8,9,10 provide data on doxorubicin levels in all the tumors subjected to FDP-NV-DOX. Small amounts of free Doxorubicin were detected in each tumor. Larger amounts of Doxorubicin were recovered from each tumor extract (Figure 8). The M-1 metabolite, doxorubicinol was identified in only 2 tumors (as the amount of the metabolite was below precise quantitation levels in 2

	Doxorubicin (free)		Doxorubicin (total)		Doxorubicinol	
Instrument	LC-MS/MS-QC_Triple Quad 6500+		LC-MS/MS-QC_Triple Quad 6500+		LC-MS/MS-QI_Triple Quad 6500+	
Analyte(s)	Doxorubicin		Doxorubicin		Doxorubicinol	
Internal standard(s)	6 in 1 internal standard in ACN (Labetalol & tolbutamide & Verapamil & dexamethasone & glyburide & Celecoxib 100 ng/mL for each)		6 in 1 internal standard in MeOH with 1% HCl (Labetalol & tolbutamide & Verapamil & dexamethasone & glyburide & Celecoxib 100 ng/mL for each)		6 in 1 internal standard in MeOH (Labetalol & tolbutamide & Verapamil & dexamethasone & glyburide & Celecoxib 100 ng/mL for each)	
MS conditions	ESI:Positive MRM detection Doxorubicin:[M+H]+m/z: 544.2 / 397.0		ESI:Positive MRM detection Doxorubicin:[M+H]+m/z: 544.2 / 397.0		ESI:Positive MRM detection Doxorubicinol:[M+H]+m/z: 546.2 / 399.1	
UPLC conditions	Mobile Phase A:0.1% FA in water Mobile Phase B:0.1% FA in ACN		Mobile Phase A:0.1% FA in water Mobile Phase B:0.1% FA in ACN		Mobile Phase A:0.1% FA & 2mM HCOONH4 in water/ACN (v:v, 95:5) Mobile Phase B:0.1% FA & 2mM HCOONH4 in ACN/water (v:v, 95:5)	
	Time (min)	Mobile Phase B (%)	Time (min)	Mobile Phase B (%)	Time (min)	Mobile Phase B (%)
	Initial	5	Initial	5	Initial	5
	1.3	50	1.3	50	1.3	50
	1.5	100	1.5	100	1.5	100
	1.8	100	1.8	100	1.8	100
	1.81	5	1.81	5	1.81	5
	1.9	5	1.9	5	1.9	5
	Column:ACQUITY UPLC HSS T3 1.8 µm 2.1 × 50 mm Column temperature:45.0°C Flow rate:0.6 mL/min		Column:ACQUITY UPLC HSS T3 1.8 µm 2.1 × 50 mm Column temperature:45°C Flow rate:0.6 mL/min		Column:ACQUITY UPLC HSS T3 1.8 µm 2.1 × 50 mm Column temperature:45°C Flow rate:0.6 mL/min	
	Retention time: Doxorubicin:1.12 min		Retention time: Doxorubicin:1.15 min		Retention time: Doxorubicinol:1.04 min	

Table 4: Summary of methodological approaches for doxorubicin and doxorubicinol analysis by LC-MS. This is the most detailed for the process known to be deposited in public domain.

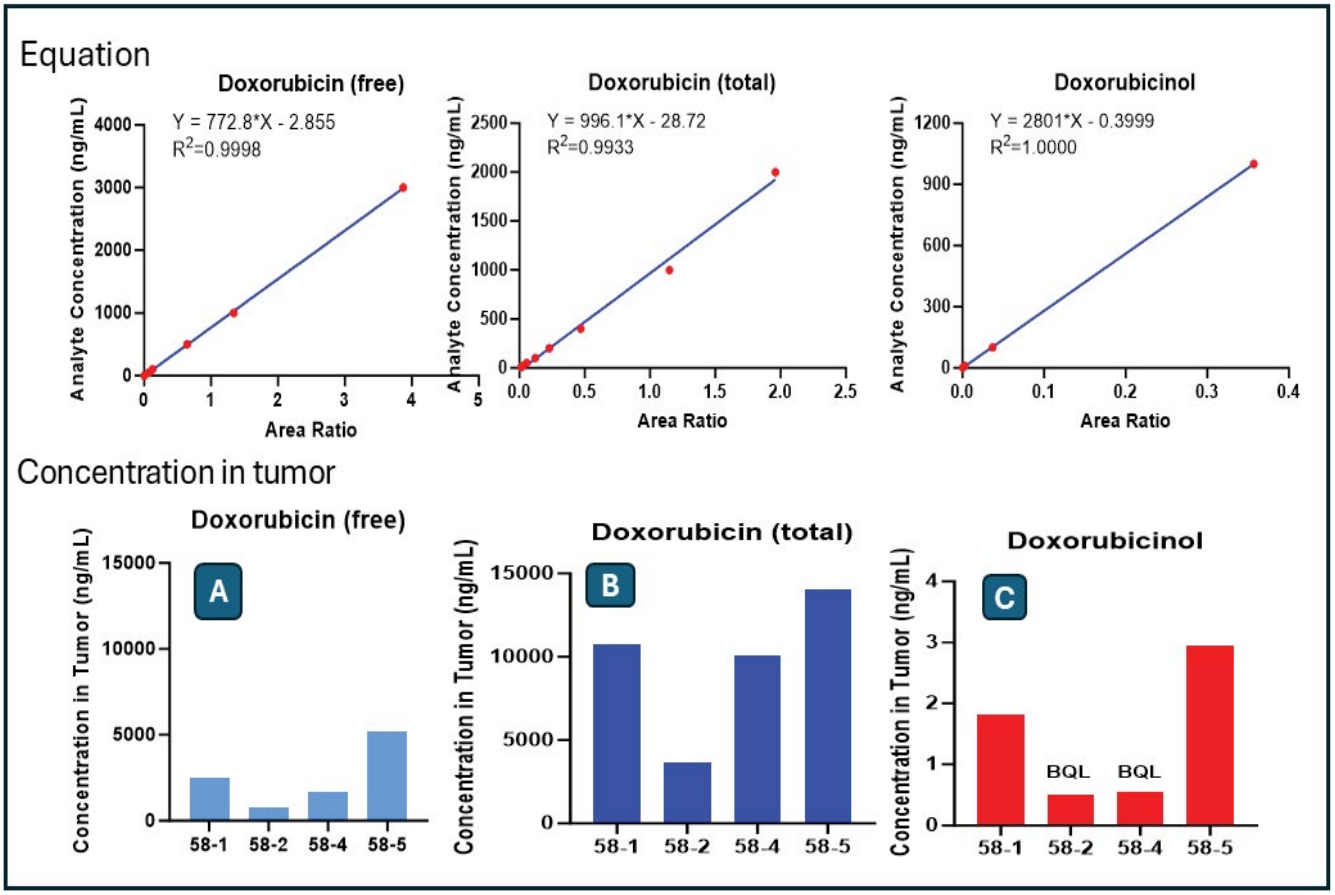

Figure 8: Upper Panel provides calibration lines for each analyte of interest. Quantitative analysis of free doxorubicin (A), and doxorubicin extracted from tumors according to protocol detailed in Table 4. of mice treated with FDP-NV-DOX-75. The upper panel Graphics presents the amount of doxorubicin and doxorubicinol in dissected tumors, analyzed by LC-MS and quantified based on the respective calibration diagrams. All specimens presented in Figure 10 and details listed in the material and methods section. Numbers under the bars represent individual animal analysis.

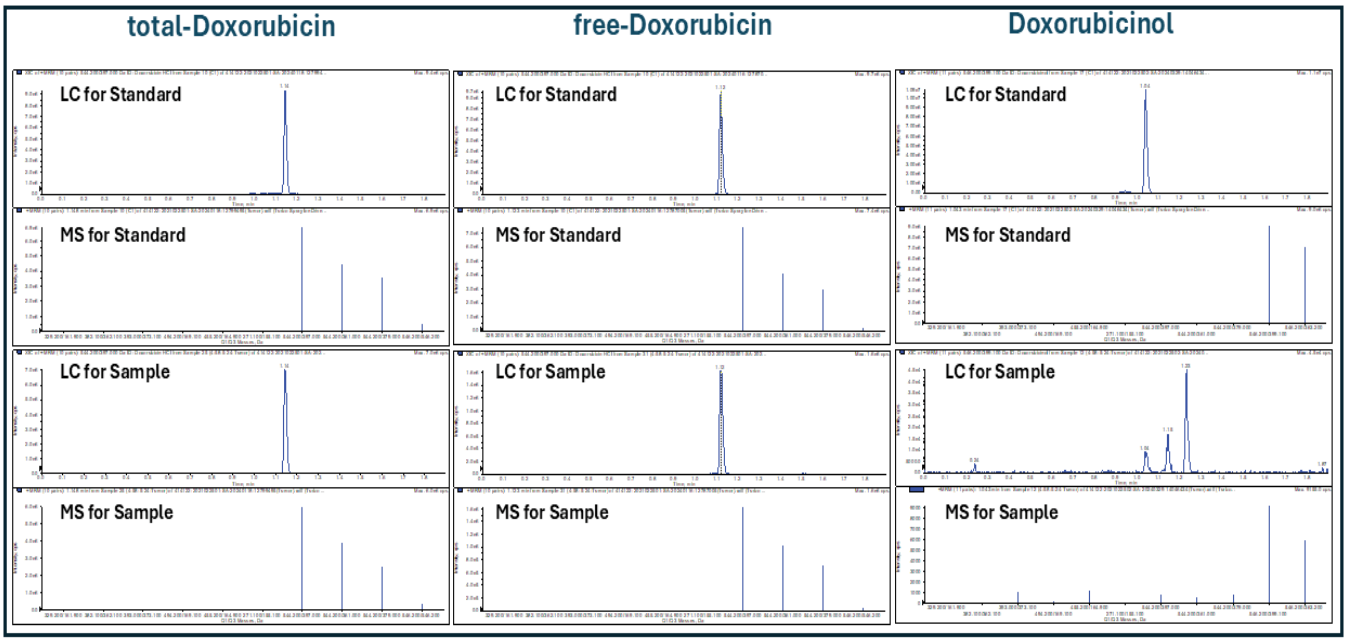

Figure 9: Represented diagrams of LC-MS analysis of doxorubicin and its metabolite doxorubicinol in dissected tumors. Highly detailed of the method of is provided in methods section.

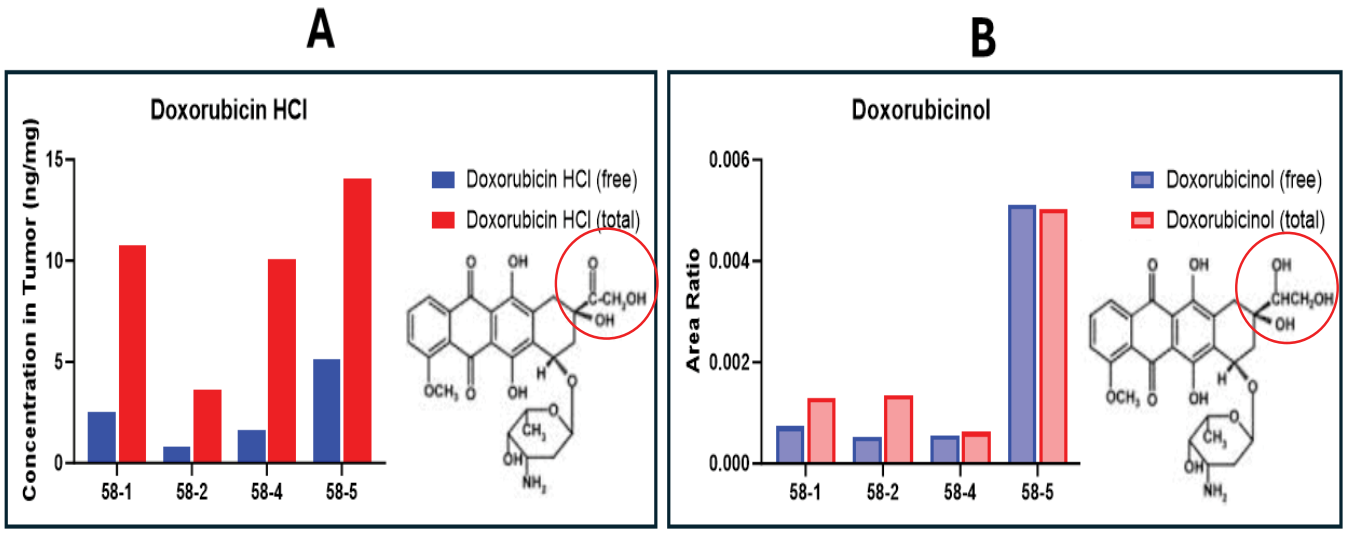

Figure 10: provides concentrations of doxorubicin extracted from the tumor (A) and doxorubicinol (B) the integrated amount of the metabolite. Red circles point out the chemical site where conversion takes place; yellow circle point out the primary amine which is protonated and facilitates in ionic interaction with the negative charge of particles; surface.

tumors out of 4 (BQL). Figure 9 reinforces the presence of doxorubicinol in tumor homogenate.

Effect of sorafenib on Hep3B-luc cells viability in vitro

Prolog: Our intension is to revoke embolectomy practice, which is the contemporary standard of medical practice. To preserve maximum efficacy, we postulated that adjuvant chemo treatments to FDP-DOX using a non-redundant drug in tandem with FDP-DOX as an adjuvant TAC (trans-arterial chemotherapy) in the earliest phase of I-HCC treatment. Sorafenib mechanism of actions interferes in multiple kinase signal transductions considered complementary to the mechanisms of DOX based on nuclear and mitochondrion function. Gerstenhaber JA et al, provides dose and time-dependent effects of sorafenib (SOR) on viability of Hep-3B-luc liver cancer cells and provides options for SOR additive to enhance FDP-DOX intra-tumor injections [36]. Furthermore, SOR suspension is intended to be delivered in its own suspension, in tandem to FDP-DOX, which is expected to virtually act instantaneously while FDP-DOX desorption lags.

Safey biomarkers: FDP-DOX impact on animal thriving and liver function tests

Biochemical functions are known to harbor biomarkers that signal adverse effects associated with systemic treatment with anthracyclines. Therefore, our efficacy studies were bundled with monitoring of animal thriving (body weight) as a systemic alarm of toxicity. Likewise, liver functions tests are established biomarkers of liver health.

None of the animals subjected to FDP-DOX treatment was excluded (via euthanasia) due to excessive body weight loss of over 20%, (as per regulatory requirements).

The impact of FDP-NV-DOX on liver functions tests are used in medical practice such as ALT (alanine trans-aminase) and AST (aspartate transaminase) among other biomarkers. In our study 2 mice were studied for LFT at the termination day of the protocol; each assay of these biomarkers (ATL and AST) no significant statistical deviation from normal levels in mice could be affirmed. LFT biomarkers trended to lower levels while risks of liver toxicities should report elevation of these biochemical markers. Moreover, tumors treated with FDP-DOX maintained body weight throughout the 52-day protocol. The summary slide is in the supplementary section.

Discussion and Perspectives

The present manuscript presents unprecedented data in support for the possibility that FDP-NV-750nm suits to serve as a carrier for drugs delivery for liver cancer and especially the intermediary stage (I-HCC.) The 5 key objectives were primarily focused on proof of technical feasibility and establishing “proof of concept” (POC) Figure 11 affirms that PDP-NV-750nm-DOX alone is indeed capable to desorb of its coating (in the case of DOX) and fast acting adjuvant (SOR) known for fast and complementary actions to the anthracyclines. The data presented in figures 1-5 unequivocally demonstrated efficacy in single (e.g. FDP-DOX) or combination (FDP-DOX+SOR) treatments. The efficacy is shown by reducing tumor growth (measured by caliper method) and decreasing bioluminescence of luciferin emission as a biomarker (reduced emission) through FDP-DOX treatment. Additional biomarkers also supported FDP-DOX effectiveness. Thus, whole-body imaging (by IVIS) illustrated high suppression of some tumors and complete cessation of tumors progression (figure 6, FDP-DOX treated tumors mouse #1 and #3 (red arrows) Furthermore, while efficacy of each treatment manifested attenuated tumor growth (to a variable extent, figure 7) and whole-body tumor volume visualized cases of complete arrest of growth.

While evidence of efficacy to attenuation of tumors’ growth or biomarkers of function (bioluminescence,)

our histology/histochemistry figures (Figure 12 and Figure 13) illustrate pathological aberrations of tumors' integrity such as destruction of tumors' microstructures including capillaries visualized by hemorrhages, necrosis. Of great interest are topographical positions of the innate cells positions to the FDP-NV-DOX particles. Figure 16 suggests possible colocalization of particles which seem to overlap with phagocytic cells (identified by CD68+ immunohistology.) Figure 14 also suggests that FDP-NV-750nm might be up taken into cells' cytosol, a possibility in line of our recent in vitro studies with Hep-3B cells where FDP-NV particles (coated or not by DOX) could be clearly identified in the cancer cells forming corona around the nuclei but no incorporation into nuclei had been vetted [36] and validated by confocal imaging. Moreover, the extent of the damage to tumors by each of the treatments (separately or in combination) Figure 14 also provides an assembly of biomarkers (FDP, DAPI/Nuclei, FDP/NIR) revealed further by histological techniques where standard stains of tumor slices are prepped for microscopy inspection. Since these slices have been prepped ex-vivo shortly after the end of the protocol, we assume that the histopathological observation must have been elicited by the chemotherapeutic agents (whether direct acting, SOR) or those desorpted from the particles over several weeks (FDP-DOX, 38-52 days). In Figure 12, four H&E-stained slices from each of the treated groups. was probed by low to high microscopy Visual inspection of slices produced from the control tumors appear to have maintained their dense clusters of tumor-cells and overall preservation of the integrity of the tumor. In summary, the proof of efficacy has been grounded by several phenomena not observed in the vehicle control tumors. The extent of efficacy of the various approaches landed different pathognomonic markers of ultimate cells death, which in combination could lead to complete arrest of the tumors (figure 7). The lowest percent growth under treatments was generated by FDP-DOX+SOR (29%) and complete arrest in cases listed in Figure 6 would likely manifest many more should FDP-DOX treatment repeated, and its adjuvant (SOR) acted in synergy from start of treatment.

Finally, figure 12 (in the supplement section) provides supplementary data from a study we performed at our CRO cancer pathology team of WuXiAppTec where FDP-NV-DOX was tested in tandem (side by side) which FDP-DOX+SOR (Figure 5). This study was the shortest protocol (38 Days) yet, the highest efficacy to suppress bioluminescence was noted for FDP-DOX+SOR, and least by FDP-DOX. Tumors from FDP-NV-DOX have been prepped for histology analysis, which has been analyzed by the end of the protocol and subjected to histological microscopy. Similar pathological markers were spotted in line of the observation reported for figure 12. Whole body imaging (IVIS) visualized the distribution of the FDP particles and tumors' silhouette. Additional histological evidence and high-density cell counts provided important evidence generated by counting, using HALO software techniques. Furthermore, direct assay of doxorubicin and its prime metabolites doxorubicinol, confirmed the presence of DOX in each of the tumors albeit in variable quantities.

The apparent synergy of FDP-DOX+SOR displayed by duplex sorafenib further augmented the efficacy of FDP-DOX, likely due to non-redundant mechanisms of actions. The extent and speed of action of FDP-DOX-SOR, should consider the limitations of the mass of the "payload"- DOX, which was a technical limitation by the amount of DOX the FDP carried. Furthermore, unlike the clinical practice, where 'cocktails" of treatment-regimens are prescribed, our *in vivo* study fell short to sustain the time course prescribed for FDP-DOX per se. Future studies are needed to test repeated

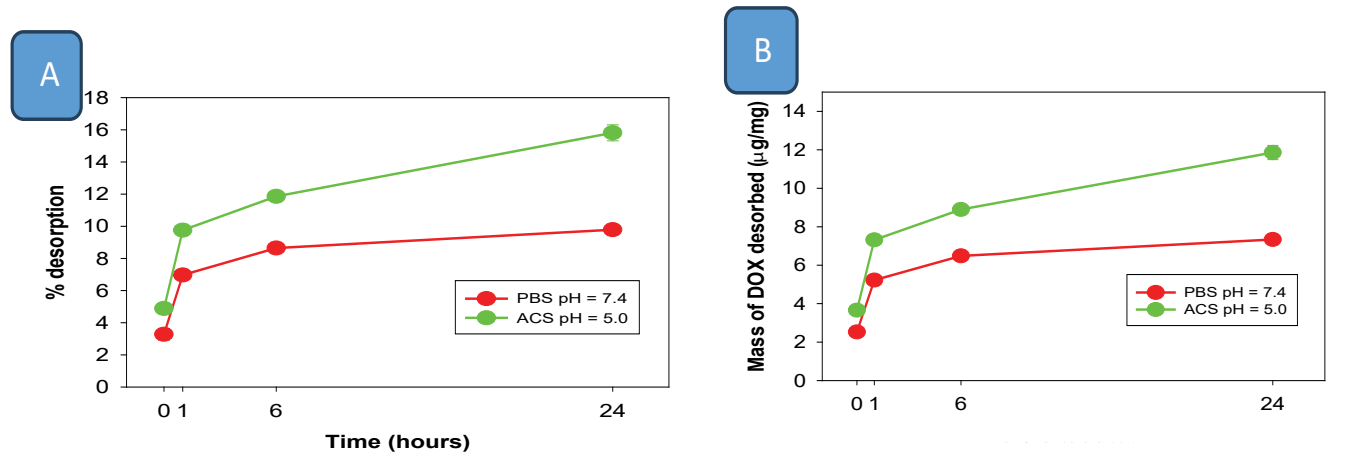

Figure 11: Desorption study of DOX from FDP-NV-750nm nm in phosphate buffered saline (PBS) pH = 7.4 and acetate buffered saline (ACS) pH = 5.0. FDP-NV-750nm with adsorbed DOX (75 µg/mg) were incubated in the buffers by 1, 6 and 24 hours and centrifuged with 16,000 x g force for 5 min. Supernatants were transferred to 96-well plate, which was measured using Tecan fluorescence plate reader with 480 nm excitation and 590 nm emission wave lengths. Amount of DOX was calculated from the standard curve prepared in parallel on the same plate from known concentrations of DOX. Error bars present SD from 3 samples prepared in separated tubes.
A) Plot presents percentage of desorption of DOX from solid phase FDP-NV-750nm into liquid phase of buffer.
B) Plot presents amount of DOX in the liquid phase of buffer desorbed from solid phase of 1 mg of FDP-NV-750 nm.

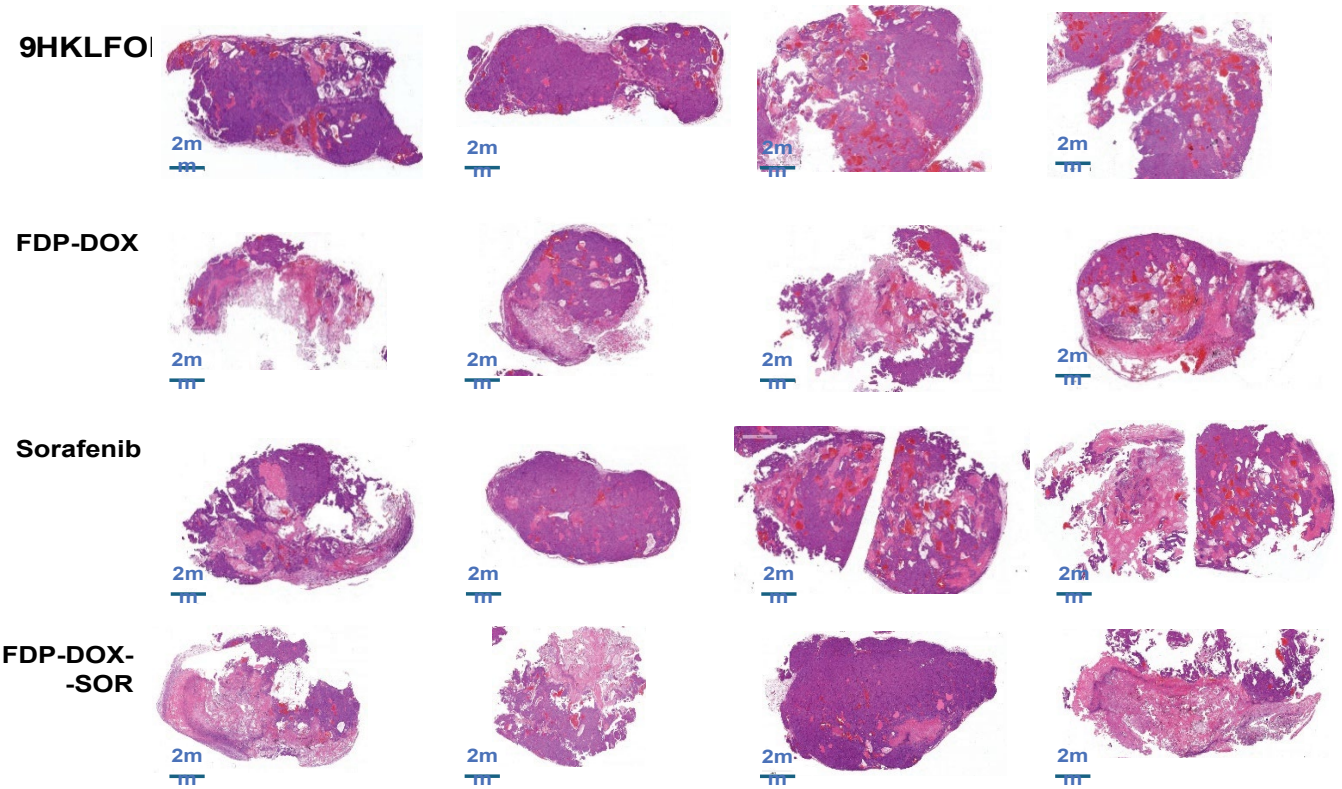

Figure 12: Each tumor from the following group: 1. Vehicle controls; 2. FDP-DOX-75, 3. Sorafenib and 4: NV -from The control slides illustrate dense masses of packed cancer cells; in contrast, most of FDP-DOX, sorafenib per se and FDP-DOX+SOR treated tumors were significantly impacted by any of these treatments. No quantitative analysis had been performed as visual inspection is clear.

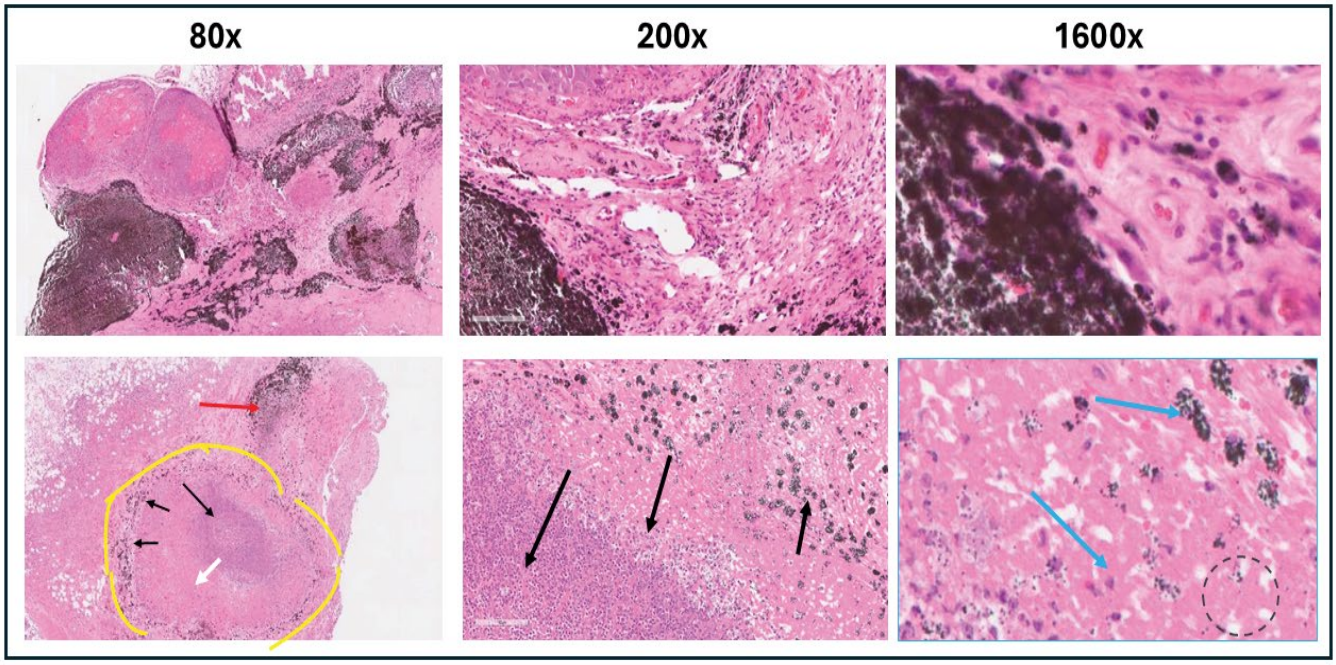

Figure 13: Representative images of paraffin sections of tumor tissue dissected on day 60 and H&E stained.
Black areas represent FDP-NV-DOX-75 accumulation.
A necrotic area was discernible (within the yellow circle), characterized by a core region with granulocyte aggregation (blue arrow). At the periphery (brown arrow), granulocyte infiltration was noted, accompanied by tumor-associated angiogenesis, where endothelial cells encircled red blood cells and granulocytes. Beyond the periphery (black arrow), certain non-tumor cells, having phagocytosed nanoparticles, exhibited no nuclear heterogeneity. The necrotic cells (white arrow or circle) displayed an indistinct morphology, complicating cell type determination. In the nanoparticle-rich region (red arrow), a substantial presence of red blood cells was observed, indicating significant hemorrhage.

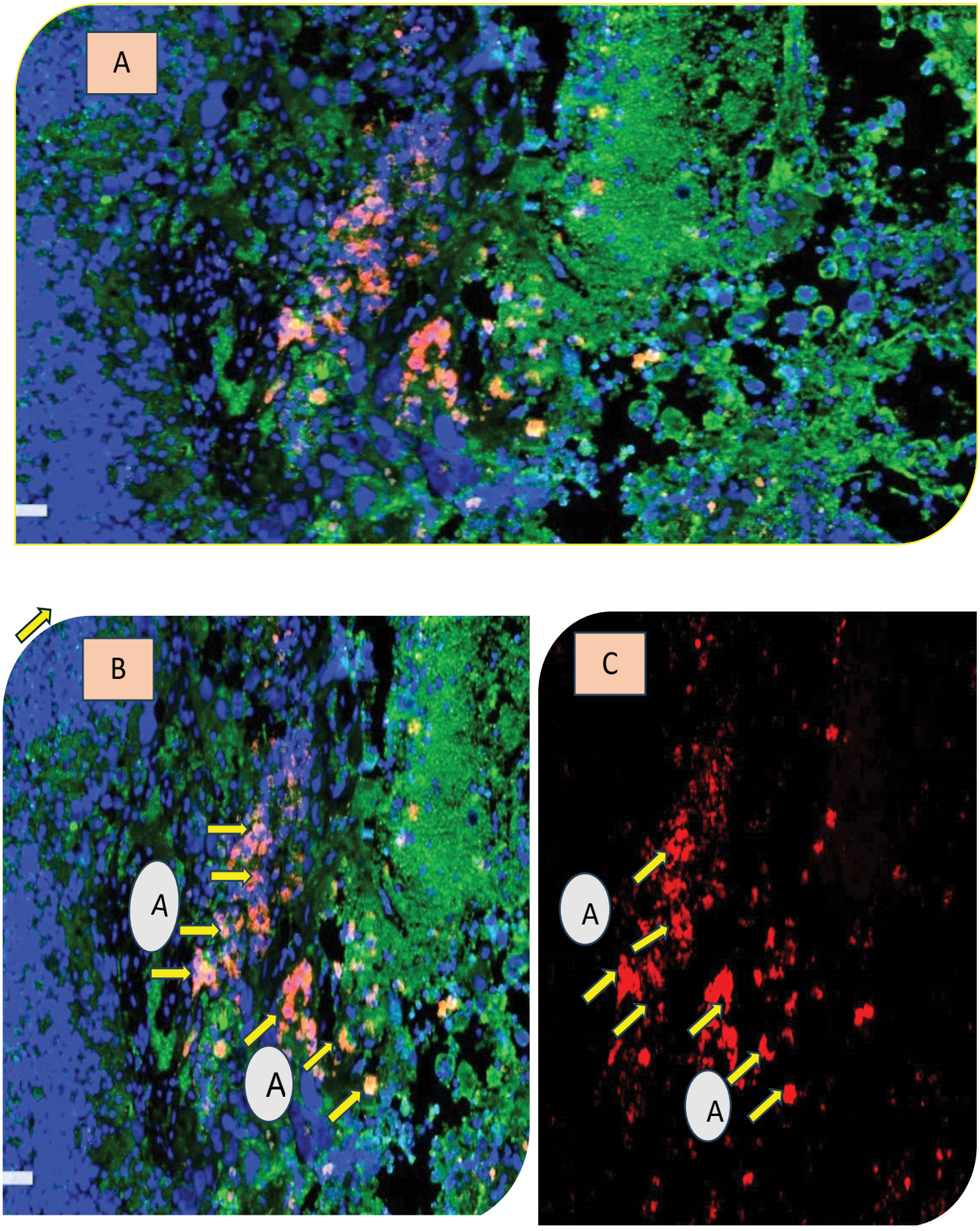

Figure 14: Part A and B illustrate the presence of immune/inflammatory cells marked by immuno-assay for $CD68^{+}$. In addition, $CD68^{+}$ cells marked by presence of phagocytic cells (stained pink) and possibly the uptake of FDP-NV-DOX into cancer cells cytosol but not into the nucleus Part C presents colocalization of FDP-NV-DOX upon activation NIR by IVIS system. The precision by which FDP-DOX colocalization (C) with CD^{68} phagocytic cells suggest that FDP-NV-DOX750 might be up taken into by cells where desorption of DOX could be accelerated by low pH of the cytosol of phagocytic cells could as well taking a role in release of free DOX which diffuses.

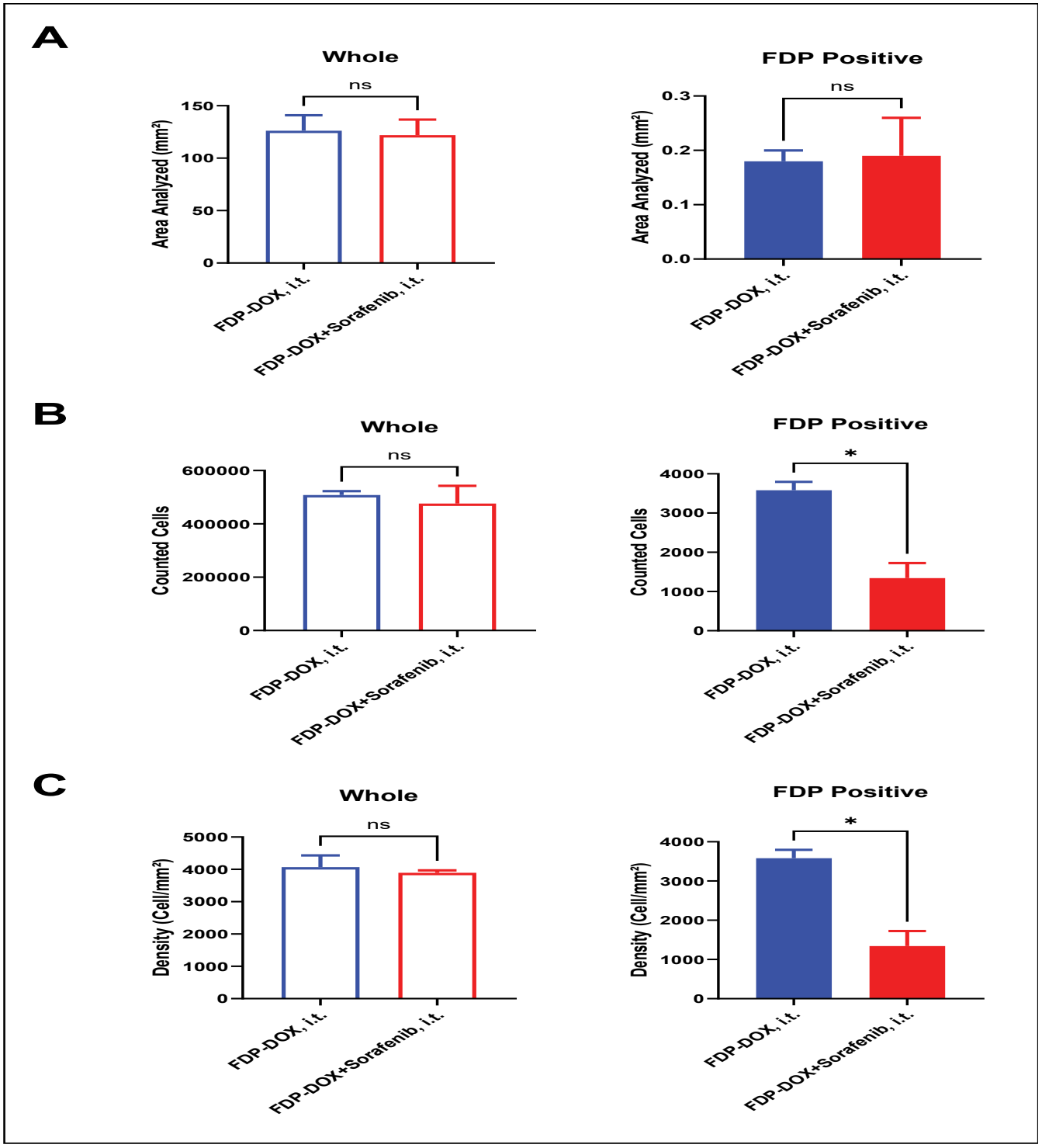

Figure 15: Tissue dimensions in the immunofluorescent stained slides were assessed using HALO software. **A),** DAPI stained spots were identified as cell nuclear, and NIR fluorescent signal indicated the FDP accumulated regions. Compared with the FDP accumulated regions from FDP-DOX treated group, less cell nuclear were observed in that from FDP-DOX + Sorafenib treated group. The size analysis and the cell number were assessed using HALO from the whole slide and FDP accumulated regions separately. The cell density was calculated as the ratio of the counted cell number to the corresponding tissue area (mm^2). Compared with the FDP-DOX, i.t. treated group, the whole area, whole cell number, and whole density of the tumors treated with FDP-DOX + Sorafenib, i.t. did not exhibit significant differences. The area of the FDP accumulated regions also showed no significant difference; however, the cell number and density in the FDP accumulated regions were reduced with statistical significance. Error bars represent SEM for two specimens per group (N = 2), T-testing between FDP-DOX, i.t. and FDP-DOX + Sorafenib, i.e. was performed by Prism.

treatment to maximize the FDP-DOX efficacy. Ultimately, the critical element for validation FDP-DOX efficacy must seek overall survival endpoints, which is the hallmark of success especially in respect to the high unmet medical needs for intermediary liver cancer.

Summary

We consider the data provided in this manuscript to satisfy the objectives set forth (vide supra) for FDP-NV-750nm prospect to serve as an efficient drugs carrier and that FDP-DOX injected directly into tumor (ultimately via trans-arterial) effectively desorb chemotherapeutics agents. Figure 15 verified "payload desorption" sufficient to deliver chemotherapeutic agent (e.g. doxorubicin) into the tumors and significantly arrest tumors' proliferation. Further in vivo studies are required to more accurately represent human biology and validate trans-arterial procedures.

Conflict of Interest

None

Acknowledgement

We wish to acknowledge Dr Francesca Vena for her support to obtain data that indicates a high correlation between MRI and Caliper monitoring of growing tumors.

We wish to acknowledge the guidance provided by Dr Zhuang Xiaoying for his assistance in developing our protocols, summarizing data and counsel on successful outcomes

References

1. McGlynn KA, Petrick JL, El-Serag HB (2021) Epidemiology of hepatocellular Carcinoma. Hepatology 73: 4-13.
2. Singal AG, Kanwal, Llovet F, Josep M (2023) Global trends in hepatocellular carcinoma epidemiology: implications for screening, prevention and therapy. Nat Rev Clin Onco 20: 864-884.
3. Rumgay H, Arnold M, Ferlay J, Olufunmilayo L, Citadel JC, et al. (2022) Global burden of primary liver cancer in 2020 and predictions to 2040. J Hepatol 77: 15981606.
4. Elshaarawy O, Gomaa A, Omar H, Rewisha E, Waked I (2019) Intermediate stage hepatocellular carcinoma: a summary review. J Hepatocell Carcinoma 6: 105-117.
5. Khanna R, Verma SK (2018) Pediatric hepatocellular carcinoma. World Journal of Gastroenterology 24: 3980-3999.
6. Sayiner M, Golabi P, Younossi ZM (2019) Disease Burden of Hepatocellular Carcinoma: A Global Perspective. Dig Dis Sci 64: 910-917.
7. Sinha MS, Stern AD, Raj AK (2024) Four decades of Orphan Drugs and priorities for the Future. NEJM 391: 100-102.
8. Conroy R (2023) Ezurpimtrostat Receives FDA Orphan Drug Designation for Liver Cancer Subtype.
9. Green CS, Bulger EM, Kwan SW (2016) Outcomes and complications of angioembolization for hepatic trauma: a systematic review of the literature. J Trauma Acute Care Surg 80: 529-537.
10. Forner A, Llovet JM, Jordi Bruix J (2012) Chemoembolization for intermediate HCC: Is there proof of survival benefit? J Hepatology 56: 984-986.
11. Llovet JM, Bruix J (2003) Systematic review of randomized trials for unresectable hepatocellular carcinoma: Chemoembolization improves survival. J Hepatology 37: 429-442.
12. Llovet JM, Real MI, Montaña X, Planas R, Coll S, et al. (2002) Arterial embolization or chemoembolization versus symptomatic treatment in patients with unresectable hepatocellular carcinoma: a randomized controlled trial Lancet 359: 1734-1739.
13. Makuuchi M, Sukigara M, Mori T, Kobayashi J, Yamazaki S, et al. (1985) Bile duct necrosis: complication of transcatheter hepatic arterial embolization. Radiology 156: 331-334.
14. Bian LF, Zhao XH, Gao BL, et al. (2020) Predictive model for acute abdominal pain after trans arterial chemoembolization for liver cancer. World Journal of Gastroenterology 26: 4442-4452.
15. He JJ, Yin XX, Wang T, Zhang S, Ge GM, et al. (2021) Factors influencing post-embolization syndrome in patients with hepatocellular carcinoma undergoing first transcatheter arterial chemoembolization. Journal of Cancer Research and Therapeutics 17: 777-783.
16. Lim HB, Kim, MS (2023) Risk Predictors of Post-Embolization Syndrome after Trans arterial Chemoembolization by Sex: A Retrospective Study. Korean Journal of Adult Nursing 35: 418-427.
17. Krishnamurthy P, Brown M, Agrawal S, et al. (2017) Acute pancreatitis as a complication of trans-arterial chemoembolization of hepatocellular cancer-case report and review of literature. J Gastrointestinal Oncol 8: E26–E30.
18. Pan CW, Bashar A, Lo CH, et al. (2023) Epidemiological Trends and Gender Differences in Hepatocellular Carcinoma: Analysis from the Global Burden of Disease Study 2019. The American Journal of Gastroenterology; 118 (10S): pS1161.
19. Kim S, Kim HY, Lee SL, Ku YM, Won YD, et al. (2020) Lipiodol Pneumonitis Following Transcatheter Arterial Chemoembolization for Hepatocellular Carcinoma. J Liver Cancer 20: 60-66.
20. Senapati S, Mahanta SK, Kumar S (2018) Controlled drug delivery vehicles for cancer treatment and their performance. Signal Transduction and Targeted Therapy 3: 7.
21. Madaan K, Kumar S, Poonia N, Lather V, Pandita D (2014) Dendrimers in drug delivery and targeting: Drug-dendrimer interactions and toxicity issues. J Pharm Bioallied Sci 6: 139-150.
22. Sairam AB, Sanmugam A, Pushparaj A, et al. (2023) Toxicity of Polymeric Nanodrugs as Drug Carriers. CS Chemical Health & Safety 30: 5.
23. Chauhan S, Jain N, Nagaich U (2020) Nanodiamonds with powerful ability for drug delivery and biomedical applications: Recent updates on in vivo study and patents with powerful ability for drug delivery and biomedical applications: Recent updates on in vivo study and patents. Review Paper. J Pharm Anal 10: 1-12.
24. Ho D, Wang CHK, Chow EKH (2015) Nanodiamonds: The intersection of nanotechnology, drug development, and personalized medicine. Science advances 1: e1500439.
25. Moore L, Grobárová V, Shen H, Man HB, Ho D, et al. (2014) Comprehensive Interrogation of the Cellular Response to Fluorescent, Detonation and Functionalized Nanodiamonds. Nanoscale 6: 11712-11721.
26. Laura Moore, Yang J, Ho D, Osawa E, Lee DK, et al. (2016) Biocompatibility Assessment of Detonation Nanodiamond in Non-Human Primates and Rats Using Histological, Hematologic, and Urine Analysis. ACS Nano 10: 7385-400.
27. Shenderova O, Shames AI, Nunn NA, Torelli MD, Vlasov I, et al. (2019) Review Article: Synthesis, properties, and applications of fluorescent diamond particles. J Vac Sci Technol B 37: 030802.
28. Merkel TJ, DeSimone JM (2011) Dodging drug-resistant cancer with diamonds. Nanodiamond-drug conjugates show antitumor activity in mouse models of chemo resistant breast and liver cancer. Sci Trans Med 3: 73ps8.
29. Man HB, Ho D (2013) Nanodiamonds as Platforms for Biology and Medicine. Translating Life Sciences Innovation. Novel Drug Development and Delivery 18: 1.
30. Francis SJ, Torelli MD, Nunn NA, Arepally GM, Shenderova OA (2023) Clot Imaging Using Photostable Nanodiamond. Nanomaterials (Basel) 13: 961.
31. Moore L, Grobarova V, Chen H, Ho D et al. (2014) Comprehensive interrogation of the cellular response to fluorescent, detonation and functionalized nanodiamonds. Nanoscale 6: 11712.

32. Zhu Y, Li J, Li W, Zhang Y, Yang X, et al. (2012) The Biocompatibility of nanodiamonds and application in drug delivery. Theranostics 2: 302-312.

33. Marcinkiewicz C, Sternberg M, Feuerstein GZ, Lelkes PI (2020) Effects of Fluorescent Diamond Particles FDP-NV-800nm on essential biochemical functions of primary Human Umbilical Vein Cells and human hepatic HepG-2 in vitro (Part VI): Acute biocompatibility studies. Nanotech, Science & App 13:103-118.

34. Firestein R, Marcinkiewicz C, Feuerstein GZ, Nie L, Chua HK, et al. (2021) Pharmacodynamic Studies of Fluorescent Diamond Carriers of Doxorubicin in Liver Cancer Cells and Colorectal Cancer Organoid. Nanotechnology, Science and Applications 14: 139-159.

35. Feuerstein GZ, Marcinkiewicz C, Firestein R. et al. (2023) Pilot Studies towards Development of Fluorescent Nanodiamonds Particles FDP-NV-700/800nm as Carriers of Doxorubicin for Imaging and Adjuvant Treatment of Hepatocellular Cancer: Part 1: Int J NanoResearch 7: 01-26.

36. Gerstenhaber JA, Marcinkiewicz C. Feuerstein GZ, Barone FC, Sternberg M, et al. (2019) Biocompatibility studies of fluorescent diamond particles-(NV)~750nm: in vitro kinetics and in vivo localization in rat liver following long-term exposure Part (V). International Journal of Nanomedicine 14: 6451-6464.

37. Reiberger T, Chen Y, Ramjiawan RR, Hato T, Fan C, et al. (2015) An orthotopic mouse model of hepatocellular carcinoma with underlying liver cirrhosis. Nat Protoc 10: 1264-1274.

38. Marcinkiewicz c, Gerstenhaber AJ, Feuerstein GZ, Sternberg M, Lelkes PI (2017) Bitistatin-functionalized fluorescent nanodiamond particles specifically bind to purified human platelet integrin receptor alpha 2b beta3 and activated platelets. International Journal of Nanomedicine 12: 3711-3720.

39. Tsirigoti C, Ali MM, Maturi V, Heldin CH, Moustakas A (2022) Loss of SNAI1 induces cellular plasticity in invasive triple-negative breast cancer cells. Cell Death Dis13: 832.

40. Gabizon A, Shmeeda H, Barenholz Y (2003) Pharmacokinetics of Pegylated Liposomal Doxorubicin. Review of Animal and Human Studies. Clin Pharmacokinetic 42: 419-436.

41. Liu YS, Ou MC, Yi-Shan, T YS, Wang CK, et al. (2015) Transarterial Chemoembolization Using Gelatin Sponges or Microspheres Plus Lipiodol-Doxorubicin versus Doxorubicin-Loaded Beads for the Treatment of Hepatocellular Carcinoma. Korean J Radiol 16: 125-132.

42. Szebeni J, Fontana JL, Wassef NM, Mongan PD, Morse DS, et al. (1999) Hemodynamic Changes Induced by Liposomes And Liposome-Encapsulated Hemoglobin In Pigs: A Model For Pseudo allergic cardiopulmonary reactions to Liposomes. Role of Complement and Inhibition by Soluble Cr1 and Anti-C5a Antibody. Circulation 99: 2302-2309.

43. Yu J, Wang L, Xie X, Zhu W, Lei Z, et al. (2023) Multifunctional Nanoparticles Codelivering Doxorubicin and Amorphous Calcium Carbonate Preloaded with Indocyanine Green for Enhanced Chemo-Photothermal Cancer Therapy. International Journal of Nanomedicine 18: 323-337.

44. Shi Q, Zhang X, Wu M, Xia Y, Pan Y, et al (2023) Emulsifying Lipiodol with pH-sensitive DOX@HmA nanoparticles for hepatocellular carcinoma TACE treatment eliminate metastasis. Mater Today Bio 23: 100873.

45. Barenholz Y (2012) Doxil®–the first FDA-approved nano-drug: lesson learned. J Control Release 162: 117-134.

46. Zhengzhou F, Saadat M, Alizadeh H, Zakeri-Milani P, Baradaran B (2019) Liposome and immune system interplay: Challenges and potentials. J Control Release 305: 194-209.

47. Rabinowitz SS, Gordon S (1991) Macrosialin, a macrophage-restricted membrane sialoprotein differentially glycosylated in response to inflammatory stimuli. J Exp Med 174: 827-883.

48. Gao G, Guo Q, Zhi J (2019) Nanodiamond-Based Theranostic Platform for Drug Delivery and Bioimaging. SMALL, 19023. WILEY-VCH Verlag GmbH & Co. KGaA, Weinheim.

49. Jiang Z, Zhang W, Zhang, Liu T, Xing J, et.al. (2022) Nanomaterial-Based Drug Delivery Systems: A New Weapon for Cancer Immunotherapy. International J Nanomedicine 17: 4677-4696.

50. Costoya J, Surnar B, kalathil AK, Kolishetti N, Dhar S, et al. (2021) Controlled release nanoplatforms for three commonly used chemotherapeutics. Molecular Aspects of Medicine 83: 101043.

51. Mintz K, Leblanc RM (1876) The use of nanotechnology to combat liver cancer: Progress and perspectives. Biochim Biophys Acta Rev Cancer 1876: 188621.

52. Saadat M, Mostafaei F, Mahdinloo S, Abdi M, Zahednezhad F, et al. (2021) Drug delivery of pH-Sensitive nanoparticles into the liver cancer cells. Journal of Drug Delivery Science and Technology 63: 102557.

53. Eichhorn ME, Ischenko I, Luedemann S, Farokhzad OC (2019) Targeted delivery of a cisplatin prodrug for safer and more effective prostate cancer therapy in vivo. Proc Natl Acad Sci Unit States Am 108: 1850–1855.

54. Nunn N, Prabhakar N, Reineck P, Magidson V, Kamiya E et al. (2019) Brilliant Blue, Green, Yellow, and Red Fluorescent Diamond Particles: Synthesis, Characterization, and Multiplex Imaging Demonstrations. Nanoscale 11: 11584–11595.

Citation: Feuerstein GZ, Firestein R, Marcinkiewicz C (2025) Development an Innovative, Contrarian and Unprecedented Theragnostic Technology based on Submicron Fluorescent Diamond Particles, FDP-NV-750NM Coated with Doxorubicin and Duplex Sorafenib. PART II: - In Vivo Proof of Hypotheses and Technical Feasibility for Direct to Tumor Injection of FDP-NV-DOX~SOR to Xenograft Tumors in Immune Compromised BALB/C2 'NUDE' Mice. Int J Nano Rech Vol: 8, Issu: 1 (01-19).